REVIEW

Progress in atherosclerotic plaque imaging

Giulia Soloperto, Sergio Casciaro

Giulia Soloperto, Sergio Casciaro, Biomedical Engineering Science and Technology Division and Nanoimaging Ultrasound Lab at National Research Council, Institute of Clinical Physiology (CNR-IFC), 73100 Lecce, Italy
Author contributions: Soloperto G and Casciaro S contributed to this paper equally.
Correspondence to: Sergio Casciaro, PhD, Biomedical Engineering Science and Technology Division and Nanoimaging Ultrasound LAB at National Research Council, Institute of Clinical Physiology (CNR-IFC), 73100 Lecce, Italy. sergio.casciaro@cnr.it
Telephone: +39-0832-422310 Fax: +39-0832-422341
Received: March 14, 2012   Revised: May 14, 2012
Accepted: May 21, 2012
Published online: August 28, 2012

Abstract

Cardiovascular diseases are the primary cause of mortality in the industrialized world, and arterial obstruction, triggered by rupture-prone atherosclerotic plaques, lead to myocardial infarction and cerebral stroke. Vulnerable plaques do not necessarily occur with flow-limiting stenosis, thus conventional luminographic assessment of the pathology fails to identify unstable lesions. In this review we discuss the currently available imaging modalities used to investigate morphological features and biological characteristics of the atherosclerotic plaque. The different imaging modalities such as ultrasound, magnetic resonance imaging, computed tomography, nuclear imaging and their intravascular applications are illustrated, highlighting their specific diagnostic potential. Clinically available and upcoming methodologies are also reviewed along with the related challenges in their clinical translation, concerning the specific invasiveness, accuracy and cost-effectiveness of these methods.

Peer reviewer: Yi-Yao Liu, PhD, Professor, Department of Biophysics, School of Life Science and Technology, University of Electronic Science and Technology of China, Northern Jianshe Road 2-4, Chengdu 610054, Sichuan Province, China

INTRODUCTION

In 2007, more than 2200 Americans died of cardiovascular diseases each day; in particular, stroke accounted for 1 in every 18 deaths, while an estimated 1 person per minute died from myocardial infarction, as reported by the latest statistics of the American Heart Association[1]. The major cause of stroke is cerebral blood vessel blockage as a consequence of atherosclerotic plaque rupture in carotid arteries; similarly, myocardial infarction is strongly related to coronary artery narrowing as a consequence of atherosclerosis[2].

Pathogenesis of the atherosclerotic plaque: Biological and functional key features

Atherosclerosis is a systemic arterial inflammatory disease initiated by the accumulation of fatty streaks within the arterial wall, which may evolve into a cholesterol-rich lesion hardened by the presence of proliferating smooth muscle cells (SMCs); these types of lesions are called atheromas[3]. Physiologically, the arterial wall consists of three layers, starting from the exterior: tunica adventitia (collagen and fibres), tunica media (SMCs and elastic fibres), and tunica intima [endothelial cells (ECs), lining the lumen of all vessels].

Mechanoreceptors on the surface of ECs sense blood-flow-induced shear stress on the arterial lumen and transmit a stimulus to the nuclei through the cytoskeleton, inducing the intracellular signalling cascade[4-6] that eventually leads to alteration in the physical properties of ECs[7]. Consequently, intravascular low density lipopro-

teins (LDL) and circulating monocytes can migrate below the intimal layer and may coalesce to form larger beds of fatty streaks, rich in cholesterol crystals. Additionally, fibres and SMCs, physiologically present where cholesterol accumulates can proliferate leading to plaque formation and growth[3].

A plaque could then develop into a fibrous cap atheroma, consisting of a large necrotic core rich in extracellular lipid, cholesterol crystals and necrotic debris covered by a fibrous cap.

The cap is constituted by SMCs in a collagen-proteoglycan matrix, with infiltrated macrophages and T lymphocytes[3]. Inflammatory cells are also present in the shoulder of the plaque, at the interface with the underlying necrotic core. Highly calcified stable lesions or the development of mural haemorrhage are possible evolutions of the fibrous cap atheroma[3]. Moreover, T cells encountering antigens, such as Oxidized LDL and cytokines, induce macrophage activation, superoxide production, up-regulation of vascular cell adhesion molecule (VCAM)-1 and protease activity, *via* up-regulation of matrix metalloproteases (MMPs) expression, favouring matrix degradation, hence the transition from stable plaque to thin fibrous cap atheroma (TFCA), which is unstable and at risk of rupture[8]. Because atherosclerosis is a systemic disease, diagnostic imaging can be used to study arteries outside the heart such as the carotid artery and aorta, which are more accessible and suitable for the limited spatial resolution of most imaging techniques; for instance, cap thickness of the TFCA is usually lower than 200 μm when it occurs in the carotid artery bifurcation and is 65 μm when found in the coronary artery[9]. Increased neovascularisation within the atherosclerotic plaque and fibrous cap is a further marker of symptomatic carotid disease. The newly formed vasculature has larger and more irregular microvessels then the physiologic vasa vasorum and may contribute to plaque instability and to the onset of thromboembolic sequelae[10]. Immature and dysmorphic microvessels are recognized as sites of vascular leakage and inflammation; nonetheless these vessels may be therapeutic targets for promoting plaque stabilization[11]. However, the vessels exhibiting TFCA do not necessarily show severe narrowing, but do have positive external remodelling[9] (Figure 1).

The latter represents a compensation strategy to restore physiological levels of blood flow velocity when intima thickness occurs. Conventionally, low shear stress regions, such as arterial bifurcations and bends, are associated with plaque formation, whereas localized high shear stress has been linked to plaque rupture[12,13]. Nonetheless, evidence of plaque rupture occurring in a region of extremely low wall shear stress located downstream of the throat of a stenotic carotid bifurcation[14,15] contributes to undermine the consensus regarding the conventional association between shear stress values and plaque vulnerability; recent studies converge on the hypothesis that vulnerability is related to the mechanical Von Mises stress (typically five orders of magnitude larger than wall shear stress) borne by the fibrous cap, to its thickness, to arterial remodelling and to the morphological distribution of the necrotic core and other plaque components[16]. Moreover, biomechanical studies have shown that intimal tears in coronary arteries often occur at the interface of calcified and adjacent to non-calcified arterial tissues[17], thus it is likely that calcification plays an active role in plaque rupture.

Different methodologies have been developed to directly image atherosclerosis, either invasively or non-invasively. In 1959, Sones *et al*[18,19] performed the first selective coronary angiography, and this rapidly became the technique of choice for enabling the operator to observe narrowing in the arterial lumen and clinically assess the effects of atherosclerosis. However, angiography is an exclusively luminographic technique, providing no information on the extent of the disease in the arterial wall. For this reason, computed tomography (CT) and positron emission tomography (PET) are required to investigate the lesion composition. Both techniques involve ionizing radiation, potentially producing biological side effects with different classes of clinical features. Later developments in diagnostic imaging techniques, such as B-mode Ultrasound and magnetic resonance imaging (MRI), allow non-ionizing imaging of the arterial wall and eventually the assessment of its pathological status. The diagnostic imaging techniques employed for atherosclerotic plaque analysis can be graded on their level of invasiveness (Figure 2), and in this review, they are presented from the less hazardous to the most health threatening.

NON INVASIVE ATHEROSCLEROTIC PLAQUE ASSESSMENT

Non-invasive assessment of atherosclerosis targets populations at risk of cardiovascular disease and asymptomatic patients who have not yet presented with an acute cardiovascular event. Completely non-invasive diagnostic imaging modalities are those examinations performed without percutaneous access to the vessel and employing non-ionizing radiation. Non-ionizing radiation is described as a series of energy waves of different nature, such as oscillating electric or magnetic fields, sound waves and includes the spectrum of ultraviolet, visible light, infrared, microwave, radio frequency (RF), and extremely low frequency. The crucial morphological and biological features that characterize atherosclerotic plaques can be specifically addressed by non-ionizing diagnostic criteria using non-invasive imaging modalities (Table 1).

Conventional and IB ultrasound

In modern clinical practice, vessel outline reconstruction is one of the most validated and employed applications of ultrasonography (US), also supported by optimized tracking devices; in particular, because of their accessibility, carotid arteries represent the ideal site for clinical examinations[20]. In addition, the increase in intima-media thickness (IMT) of the common carotid artery can be a
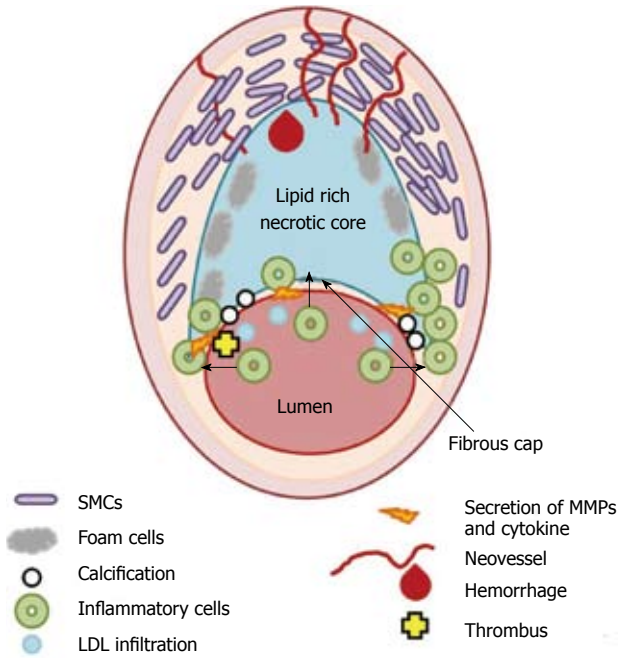
Figure 1 Scheme of the thin fibrous cap atheroma. Main cellular components characterizing atherosclerotic plaque formation and destabilization are illustrated as well as biological and morphological features occurring in vulnerable plaque. SMCs: Smooth muscle cells; LDL: Low density lipoprotein; MMPs: Matrix metalloproteases.

Table 1 Plaque feature identification through non-invasive diagnostic imaging (without using ionizing radiation)

|	US	CE-US	MRI	CE-MRI
Morphology features				
Outward remodelling	_1	_1	_1	_1
Plaque burden	_2	[39]1	_1	_1
Lipid pool	[32]1	_2	[50]1	[57]1
Necrotic core	[30]1	_2	[53]1	
Composition				
Fibro-fatty	_2	_2	[50]1	[57]1
Fibrous plaque	[32]1	_2	_1	_1
Dense calcium	[32]1	_2	[50]1	[58]1
Biological features				
Inflammation	_2	[39]1	[57]1	[60]1
Macrophage infiltration			_2	
Neo-angiogenesis	_2	[36]1	_2	[59]1
TFCA	_2	_2	[50]1	[142]1
TFCA + MI	_2	_2	_2	_2

[1]Limited clinical experience; [2]research in progress. US: Ultrasound; CE-US: Contrast-enhanced ultrasound; MRI: Magnetic resonance imaging; CE-MRI: Contrast-enhanced magnetic resonance imaging; MI: Macrophage infiltration; TFCA: Thin fibrous cap atheroma.

consequence of arterial aging and hypertension and may identify with one of the earliest stages of atherosclerosis, as large IMT is associated with cardiovascular and total mortality risk[21] and could predict cardiovascular events in patients with coronary artery disease[22] as well as in asymptomatic patients[23]. IMT is usually measured manually on longitudinal B-mode ultrasound images, but many computer-based techniques for IMT measurement have been proposed to overcome the limits of manual segmentation and measurements, most requiring a certain degree of user interaction[24-26]. Despite the widespread use of carotid IMT, it provides only limited information about the atherosclerotic process occurring distally, i.e. at the bifurcation or at the internal carotid, under different hemodynamic conditions. The latter are evaluated using Multigate Doppler systems in order to provide accurate estimates of the distribution of spectral Doppler components within human arteries, and real-time processing of all the echo signals produced along an M-line is also possible[27,28]. M-mode ultrasound records motion of the interfaces toward and away from the transducer, hence real-time measurement of arterial wall distension can be analysed through specific 2-D autocorrelation algorithms, whose results can be displayed in real-time to enhance the accuracy of diagnosis even over long acquisitions[29].

Although preliminary attempts at tissue characterisation from conventional B-mode US were conducted with encouraging high retrospective accuracy[30], the introduction of advanced analysis of the backscattered US signal, namely integrated backscatter (IB) analysis, enabled the different plaque components to be distinguished based on their specific spectral content[31]. Integrated backscatter ul-

trasonography (IB-US) methodologies allow non-invasive evaluation of the tissue substructure in human plaques by means of offline data processing techniques, that improve the poor spatial resolution on conventional US up to 300 μm. Compared with histology, the sensitivity and specificity for detecting thrombi, lipid pools and fibrous tissue ranged between 80%-85% and 78%-91%, respectively, with peak accuracy in the detection of calcified regions (sensitivity: 89%; specificity: 91%) (Figure 3)[32].

Contrast-enhanced ultrasound
Based on clinical observations and published reports, the presence of neovascularisation, characterized by high permeability, appears to be a distinct marker of plaque instability and vulnerability[10,33]. Contrast-enhanced ultrasonography (CE-US) relies on the detection of acoustic signals produced by microbubbles that are targeted to the sites of disease. Because they contain gas and are smaller than the wavelength of ultrasound, these agents undergo volumetric oscillation in an acoustic field, thereby compressing and expanding according to the acoustic pressure peaks and nadirs, respectively[34]. To improve *in vivo* stability, ultrasound contrast agents commonly contain inert gases that have low diffusion and low solubility coefficients in blood. CE-US techniques may serve to characterize intra-plaque angiogenesis[35], which is unrelated to the degree of stenosis[36]. Specifically, a retrospective study of 147 patients with symptomatic carotid atherosclerosis demonstrated how the presence and degree of adventitial vasa vasorum and plaque neovascularisation were directly associated with cardiovascular diseases and events, and could be assessed by means of contrast-enhanced ultrasound[37] down to the scale of the microvessel[38]. Additionally, a preliminary report suggests that microbubbles may also be useful in quantifying plaque inflammation within the plaque[39].
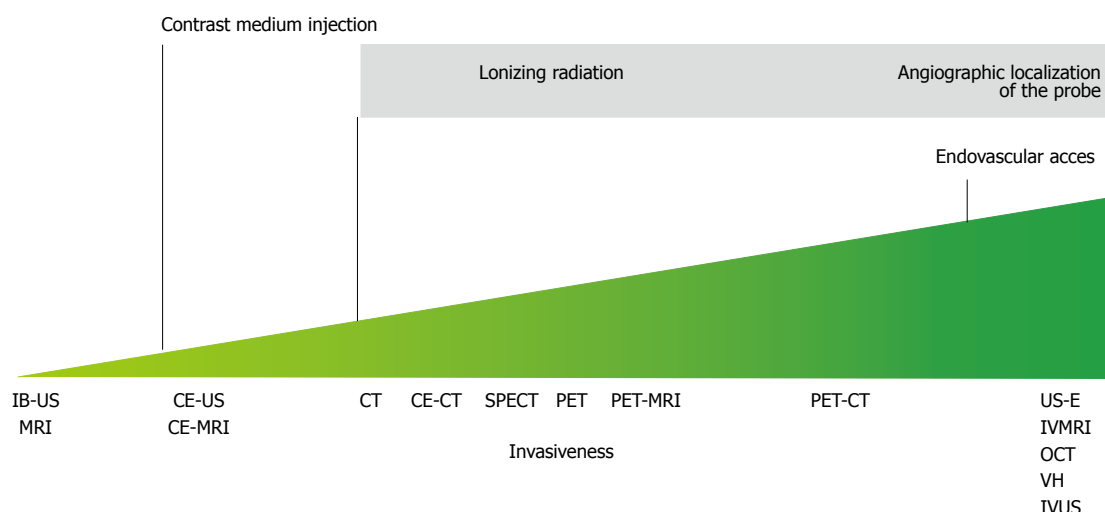
Figure 2 Illustration of the invasiveness of the possible plaque imaging modalities along with the reasons of their grading. MRI: Magnetic resonance imaging; IB-US: Integrated backscatter ultrasound; CE-US: Contrast enhanced ultrasound; CE-MRI: Contrast enhanced magnetic resonance imaging; CT: Computed tomography; CE-CT: Contrast enhanced computed tomography; SPECT: Single proton emission computed tomography; PET: Positron emission tomography; US-E: Ultrasound elastography; IVMRI: Intravascular magnetic resonance imaging; OCT: Optical coherence tomography; VH: Virtual histology; IVUS: Intravascular ultrasound.
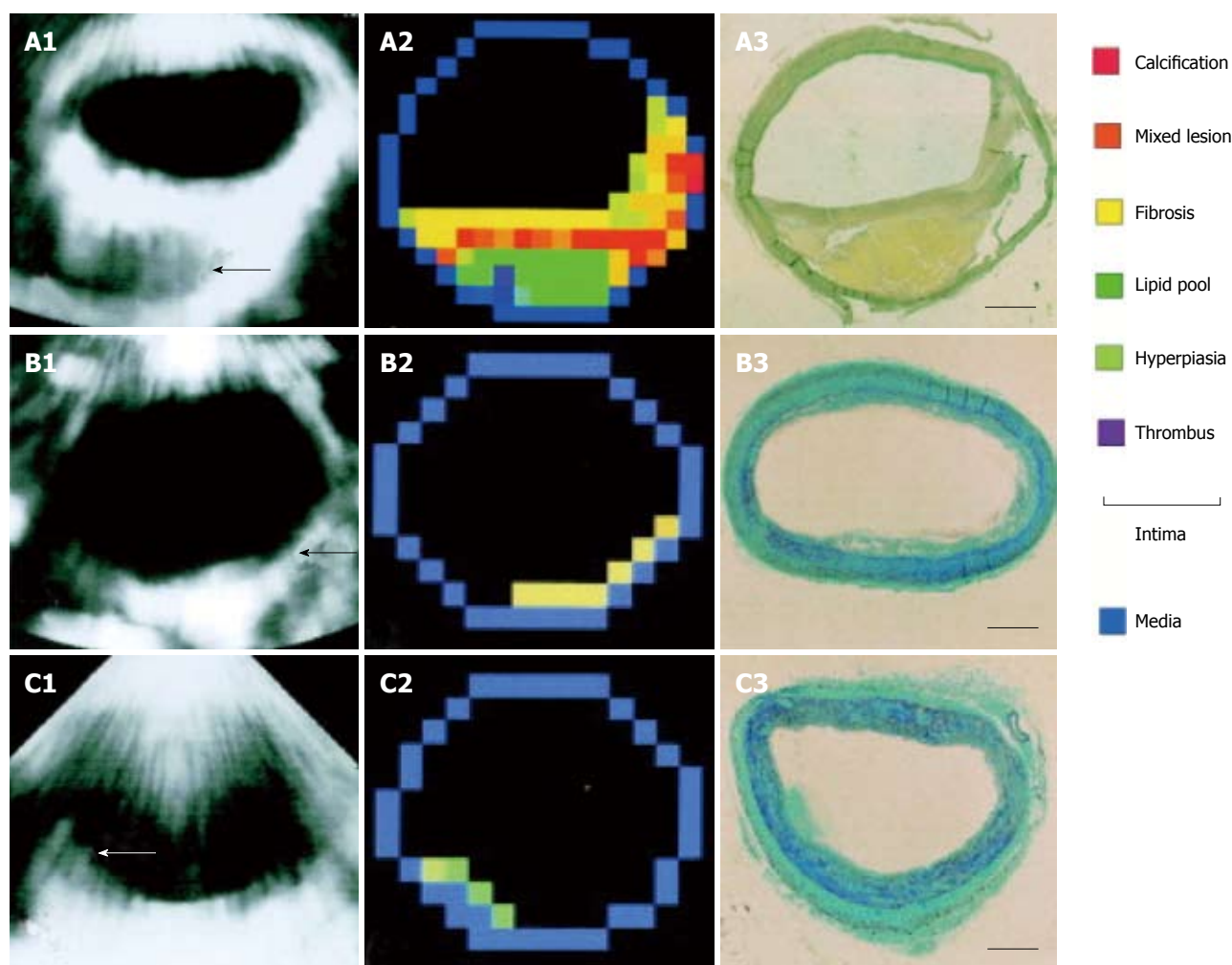
Figure 3 Example of plaque characterization trough integrated backscatter ultrasonography. A: Large plaque (arrow); A1: An integrated backscatter (IB) image at autopsy; A2: A color-coded map constructed from A1, based on the five IB categories and conventional 2D echo findings; A3: van Gieson staining of the same segment as the IB measurement (bar = 1 mm); B: Intimal fibrosis (arrow); B1: An IB image during life; B2: A color-coded map constructed from B1; B3: Masson's trichrome staining of the same segment; C: Intimal hyperplasia consisting of smooth muscle cells (arrow); C1: An integrated backscatter image during life; C2: A color-coded map constructed from C1; C3: Masson's trichrome staining of the same segment (reprint with permission)[32].

| T2W | PDW | T1W | TOF | HE | HE | Mallory's trichrome |
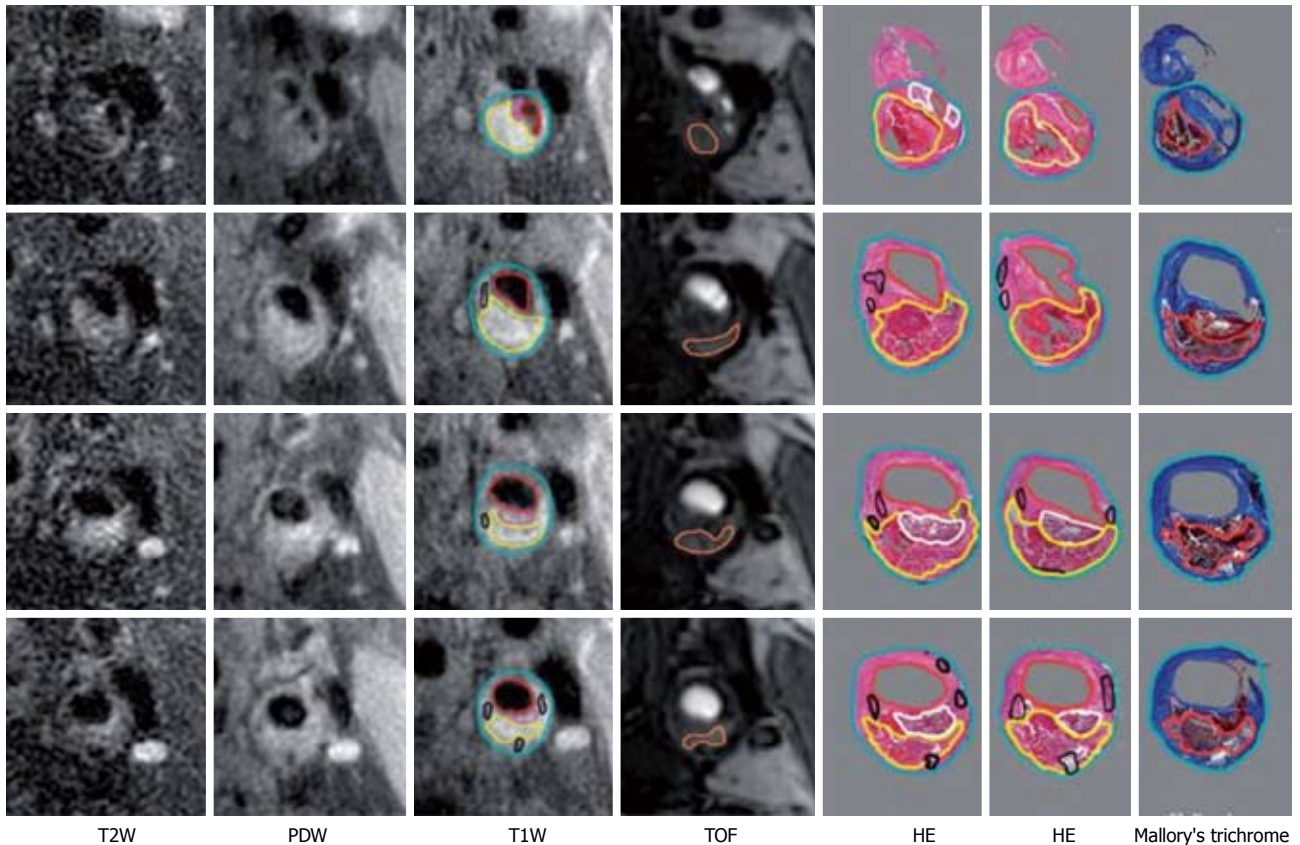
Figure 4 Example of histological validation of magnetic resonance imaging at four consecutive locations spanning the bifurcation. Multiple histological sections (at 0.5-1.0 mm-separation) generally correspond to each 2-mm thick image. Contours have been drawn for lumen (red), outer wall (cyan), lipid-rich/necrotic core (yellow), calcification (black), loose fibrous matrix (pink/white) and hemorrhage (orange)[49]. TOF: Time-of flight; HE: Hematoxylin and eosin; PDW: Proton density weighted; T2W: T2-weighted; T1W: T1-weighted.

Different US contrast agents, such as echogenic immunoliposomes (ELIP) conjugated with different proteases, have also been employed for the *in vivo* imaging of specific molecular expression in swine with induced endothelial lesions. The selective enhancement of endothelial injury/atheroma components in the presence of the functionalized ELIPs was confirmed by immunohistochemistry staining[11]. Thrombus-targeted microbubbles for CE-US conjugated with tirofiban - a glycoprotein Ⅱb/Ⅲa antagonist - can specifically bind to activated platelets in the thrombus; the capability of enhancing both the image contrast and thrombolysis, obtained as an effect of microbubble US cavitation, has been investigated with good results compared to the non-bound contrast agent[40]. Recent developments in nanoparticles (NPs) have demonstrated their potential higher safety, due to their physical stability, and the same molecular specificity; in particular, low dose silica NPs are detectable with high sensitivity in experimental studies[41,42].

MRI
MRI of atherosclerosis can provide information on both plaque volume and composition in the different arterial districts. Recent developments in coil and MRI sequence design[42,43] allow *in vivo* imaging of carotid artery plaques with a spatial resolution of 300 μm at 1.5 Tesla[44,45]. Additionally, the introduction of multispectral imaging allowed the characterisation of pathological plaque components (Figure 4), discrimination of the lipid core, the fibrous cap, calcification, haemorrhage and thrombus with sensitivity and specificity values of 76%-92% and 65%-86%, respectively[46-50]. Direct thrombus imaging is possible with specially optimized T1 weighted magnetization-prepared 3-dimensional rapid acquisition gradient echo (MP-RAGE) sequences, that comprise an inversion recovery RF pulse for magnetization preparation and a fast gradient echo acquisition sequence[51]. With the inversion time properly selected, a strong T1 weighting can be achieved, effectively detecting haemorrhage as proved in clinical studies[52].

A new slab-selective phase-sensitive inversion-recovery (SPI) technique is also promising improvements in the imaging of intraplaque haemorrhage[53]. SPI sequences were compared with MP-RAGE and evaluated both *ex vivo* and *in vivo* for discriminating intraplaque haemorrhage and arterial wall; SPI had better intraplaque haemorrhage identification accuracy ($P < 0.01$) and a significantly higher intraplaque haemorrhage-wall contrast-to-noise ratio than MP-RAGE[53]. Further examples of clinical results of MRI plaque imaging application in symptomatic patients with different degrees of carotid stenosis were provided in a study of the association between plaque characteristics, cardiovascular risk factors and statin use by means of plaque 1.5-T MRI (sequences

used were: 3-dimensional T1-weighted turbo field echo, 3-dimensional time-of-flight, 2-dimensional T2-weighted turbo spin-echo, and pre- and postcontrast 2-dimensional T1-weighted turbo spin-echo images). Statin use was positively associated with the percentage of fibrous tissue within the plaque, and evidence suggests that symptomatic patients with moderate stenosis have a higher prevalence of complicated plaques than patients with mild stenosis[54]. The use of higher magnetic field strength for evaluating possible atherosclerotic plaque progression is also documented. In particular, a cohort of patients with symptomatic and asymptomatic carotid plaques, presenting with recent intraplaque haemorrhage, underwent 3.0-Tesla MRI over a period of 18 mo[55]. MR sequences included three-dimensional time-of flight (3D-TOF), quadruple-inversion-recovery T1WI (QIR-T1WI), proton density-weighted imaging (PDWI), and T2-weighted imaging (T2WI). The contrast-to-noise ratio of intraplaque haemorrhage showed a significant difference between the haemorrhages found in symptomatic and asymptomatic carotid plaques on 3D-TOF ($P = 0.029$), QIR-T1WI ($P = 0.005$), and PDWI ($P = 0.028$), but not on T2WI ($P = 0.362$). Symptomatic intraplaque haemorrhage displayed no significant change in signal intensity, whilst asymptomatic intraplaque haemorrhage contrast-to-noise ratios exhibited a gradual decreasing trend on all contrast weighted images ($P < 0.05$). Repeat carotid intraplaque haemorrhage may be more common in patients with symptomatic than asymptomatic plaques and could represent a possible stimulus for progression of atherosclerosis which is stronger than one-time carotid intraplaque haemorrhage[55].

Contrast-enhanced MRI

Contrast-enhanced MRI (CE-MRI) is typically used to perform magnetic resonance angiography (CE-MRA); CE-MRA can be supplemented with time-resolved angiography, flow measurement, vessel wall imaging, and plaque characterisation for a more comprehensive assessment of vascular diseases[56]. The two types of contrast agent suitable for CE-MRI are the paramagnetic gadolinium chelates and ultra-small super paramagnetic iron oxide (USPIO) particles; however, some patients exhibit adverse reactions to these agents. The standard contrast agent is Gadolinium bound to a chelate in order to obtain a biocompatible compound. Gadolinium is a rare earth metal; it has a short T1 time constant, which promotes relaxation of water molecules in its proximity, leading to high signal intensity on T1 weighted sequence. After injection, the contrast agent initially remains in the vascular space; subsequently Gadolinium-chelate moves into the extracellular space, becoming more concentrated in areas where the extravascular space is expanded, such as in scar tissue, or the fibrous cap. Intravenous Gadolinium contrast can be used to improve tissue characterisation between the fibrous cap and the lipid core (correlation coefficient: 0.87)[57,58] and to identify sites of neoangiogenesis (correlation coefficient: 0.67)[59].

Moreover, lipoproteins have been adopted for use as effective molecular imaging probes, as ApoA-I has been extracted from human plasma and reconstituted with a Gadolinium chelate; when injected into ApoE knockout mice, a significant accumulation of this particle was seen in the aorta[60]. Further potential of diagnostic imaging of plaque biological activity includes the visualisation of MMPs expression, as they contribute to destabilizing plaques by segmental remodelling; protease expression can be studied by employing an activated near-infrared fluorescence probe (99mTc-labelled annexin A5)[61] and a Gadolinium-coupled matrix metalloprotease inhibitor (MPI) (99mTc-MPI)[62]. Investigations conducted on apoE null mice of different ages, which were administered 2 tracers, demonstrated that between 20 and 40 wk the aortic lesion area increased, the disease extended into the carotids and the MMP expression was greater than apoptosis as the disease progressed. Thus, differences found in the histology correlated with differences in tracer uptake, and the results supported the premise that radiolabeled MPI is better than annexin A5 for the imaging of more advanced disease[63].

USPIO particles are iron-based blood pool agents with a strong T1 and T2 shortening effect. USPIOs have the combined property of being taken up by macrophages, and of being visible by CMR, as iron particles cause low signal intensity on CMR images. High sensitivity and specificity of CMR to USPIOs have been demonstrated by a surgical trial in which USPIOs were administered before and after endarterectomy ($P < 0.001$, sensitivity: 92.5%; specificity: 64%)[64], and USPIO-related signal drop out was concordant with plaque inflammation, as visualised by 18FDG PET (see section below), but not necessarily unlinked to the degree of stenosis[65]. Additionally, USPIOs have been used to show a reduction in carotid plaque morphology in response to intensive cholesterol lowering with statin treatment[66]; nonetheless, this agent (Sinerem® 20 mg/mL) has now been withdrawn. Larger microparticles of iron oxide (4.5 μm diameter) have also been constructed to target endothelial P-selectin and VCAM-1 adhesion molecules, which allow binding to the arterial wall in the early stages of plaque development[67].

IONIZING IMAGING TECHNIQUES

CT and PET are imaging techniques that have to compromise with the radioactivity induced by X-ray and radionuclides, respectively. Ionizing radiation may interfere with molecule binding and alter DNA and RNA transcription, generating free radicals. For instance, radiation doses associated with commonly used CT examinations resemble doses received by individuals in whom an increased risk of cancer was documented[68,69]. In Table 2, the possibilities of biological/morphological target identification of each ionizing diagnostic criterion are presented, according to the relevant literature.

Electron-beam CT and multiple detector CT

Two types of CT scanner can be used to assess athero-

Table 2 Plaque feature identification through non-invasive diagnostic imaging (using ionizing radiation)

	MDCT	CE-CT	PET	SPECT
Morphology features				
Outward Remodelling	[72][1]	[79][2]	-[2]	-[2]
Plaque Burden	-[2]	-[2]	-[2]	-[2]
Lipid pool	[77][1]	-[2]	-[2]	-[2]
Necrotic core		-[2]	-[2]	
Composition				
Fibro-fatty	[77][1]	[80][2]	-[1]	-[2]
Fibrous plaque	[77][1]	[2]	-[2]	-[2]
Dense calcium	[72][1]	[2]	-[2]	-[2]
Biological features				
Inflammation	-[2]	[81][2]	[105][1]	[103][2]
Macrophage infiltration	-[2]	[2]		[99,100][2]
Neo-angiogenesis	-[2]	-[2]	[99][1]	-[2]

[1]Limited clinical experience; [2]research in progress. MDCT: Multidetector computed tomography; CE-CT: Contrast-enhanced computed tomography; PET: Positron emission tomography; SPECT: Single proton emission tomography.

sclerosis: electron-beam CT and multiple detector CT (MDCT). The former uses tungsten rings to generate X-ray images at 3-mm slice thickness and is used to calculate coronary artery calcium score in the assessment and prediction of cardiovascular risk[70]. Conversely, the latter uses a continuously rotating X-ray source able to obtain 0.5-mm slices during a single patient breath-hold. Intravenous contrast can be used to perform coronary angiographic (CTA) imaging in order to extract information on atherosclerotic plaques in the coronary arterial wall.

Analyses of CT imaging revealed how the amount of coronary calcium detected was correlated with the amount of coronary atherosclerosis present on histology[71], thus artery calcium scoring has been the predominant method of risk assessment using CT to date. However, the imperative to image the vessel wall, has led to an improvement in the use of CT to perform CTA in order to identify Glagov-type outward arterial remodelling ($P < 0.01$; sensitivity: 100% specificity: 90% compared to intravascular ultrasound (IVUS)[72] and to assess soft (non-calcium containing) atherosclerotic plaques. A recent study found that patients affected by plaques accompanied by positively remodelled coronary segments and characterised by CT low attenuation were at higher risk of acute coronary syndrome than were patients without these findings[73]. In younger patients, CTA can detect both calcium- and lipid-rich plaques; in elderly patients, it allows exclusion of the presence of a flow-limiting stenosis even if the calcium burden is high[74]. In addition to exquisite delineation of arterial wall calcium, CT can potentially differentiate between lipid-rich and fibrous plaque, although the overall specificity is lowered by the large overlap in the attenuation values of these plaque components[75].

However, the majority of clinical research to date has been performed employing 64-slice CT scanners; ongoing technical developments are likely to increase the ap-plicability of CT in the future. Progressive improvements introduced in MDCT imaging include the reduction of the potential for cardiac and respiratory motion artefact, as well as the introduction of 256- and 512-slice scanners aiming to significantly improve the spatial resolution[76,77] with potential for fibro-fatty plaque identification[78].

Contrast-enhanced MDCT
Detailed imaging of plaque morphology can also be performed when an appropriate contrast medium is used: a good correlation between contrast-enhanced MDCT (Solutrast 300, 300 mgI/mL^{-1}, Altana, Konstanz, Germany) and IVUS has been demonstrated in terms of plaque characterisation and volumetric analysis. The mean cross-sectional areas of plaque, lumen and external elastic membrane, and the degree of vessel obstruction (percentage of the external elastic membrane cross-sectional area occupied by the plaque) determined by IVUS and 64-slice contrast-enhanced MDCT were highly correlated ($r = 0.73$, $r = 0.81$, $r = 0.88$, and $r = 0.61$, respectively)[79]. Additionally, these findings are supported by a study investigating the possibility of constructing a MDCT based "plaque map" from a series of 0.4 mm thick cross-sectional images of the coronary artery obtained at intervals of 5 mm. Compared with the results for IVUS in the analysis of 662 slices of 78 vessels, the "plaque map" showed sensitivies of 92%, 87% and 89% in the identification of soft, intermediate and calcified lesions, respectively[80].

Macrophage accumulation can also be detected by means of iodine-based contrast agent (N1177) in combination with MDCT. The intensity of the enhancement detected with CT in the aortic wall of rabbits injected with N1177 correlated with inflammatory activity evaluated with ^{18}F-FDG PET/CT and macrophage density on histology[81].

Newly developed contrast media can also be employed in the assessment of plaques using an experimental CT scanner, such as the spectral CT system, in which incident X-rays are divided into six different energy bins to achieve multicolour CT imaging. Different compounds were imaged in a variety of phantoms: gold high-density lipoprotein nanoparticle contrast agent (Au-HDL) targeting atherosclerosis, an iodine-based contrast agent and calcium phosphate[82]. Au-HDL was intravenously injected at baseline; the calcium phosphate contrast material was injected 24 h later and the CT imaging was then performed. Multicolour CT imaging, conducted with the spectral CT scanner, allowed differentiation of Au-HDL, iodine-based contrast material, and calcium phosphate in the phantoms. Multicolour CT, used in combination with Au-HDL, was further studied to evaluate its potential in characterising macrophage burden, calcification, and plaque stenosis in an apolipoprotein E knockout (apo E-KO) mouse *in vitro* model of atherosclerosis and validated against transmission electron microscopy and confocal microscopy of aorta sections[82]. Au-HDL accumulated in the aortas of the apo E-KO mice, while the
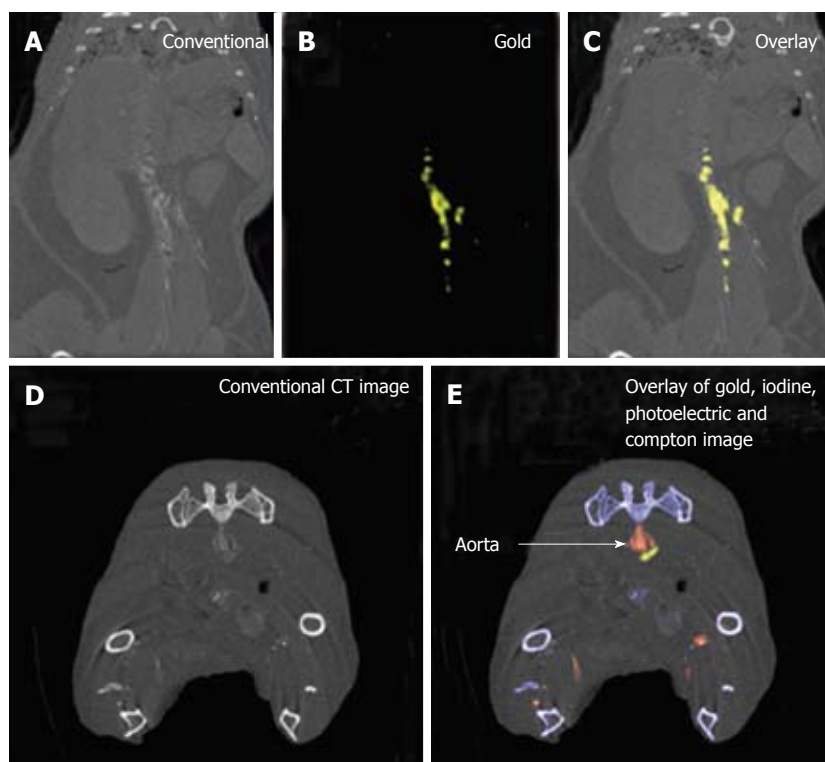
Figure 5 Example of gold high-density lipoprotein nanoparticle contrast agent detection through spectral computed tomography. A-C: Spectral computed tomography (CT) images of thorax and abdomen in apolipoprotein E knockout (apo E-KO) mouse injected 24 h earlier with gold high-density lipoprotein nanoparticle contrast agent (Au-HDL); D, E: Spectral CT images near bifurcation of aorta in apo E-KO mouse injected with Au-HDL and an iodinated emulsion contrast agent (Fenestra VC) for vascular imaging (reprint with permission)[82].

iodine-based contrast agent and calcium-rich tissue were also co-localized with the vasculature and bones (skeleton) (Figure 5).

Microscopic analysis of the samples revealed that Au-HDL is primarily found in the macrophages; hence, multicolour CT was able to image the macrophage burden. An independent review on the above study showed that if the translation of these studies to humans were successful, complete plaque characterisation would be possible by means of a one-in-all scan able to detect, simultaneously, plaque stenosis, calcification and inflammation[83]. Although multispectral CT imaging could be extremely valuable in addressing inflamed areas, the major challenge to be overcome is the high dose of gold particles administered. Specifically, tracer doses, around 35 g of Au-HDL for an adult, raise issues regarding the safety, bio-disposition, costs and consequent availability of a clinical spectral CT scanner.

However, the main concern in employing CT-based modalities is the radiation dose, which is currently between 9 and 1 mSv for a retrospectively gated MDCT coronary angiogram[84]. Recent technical advances, such as the use of volume scanning (as opposed to helical scanning) allowed a reduction in the effective radiation dose by 90% for the average examination[85]. Furthermore, the investigative use of serial MDCT plaque imaging in clinical practice is currently under optimization. Despite plaque progression being shown in the clinical setting[86], it is still unclear how this relates to patient prognosis. Conversely, a negative CT coronary angiogram has a predictive value for coronary artery disease and can avoid further invasive coronary angiography for patients at low or intermediate risk of coronary artery disease[87].

PET

PET and single photon emission CT (SPECT) are able to trace tissue metabolic activity by means of positron emitting isotopes, typically glucose isotopes bind to a tracer molecule injected into the subject. The consensus is that 18-fluorodeoxyglucose (18FDG), the most commonly used tracer, uptake is generally greater in symptomatic atheromatous plaques than in asymptomatic lesions[88] and the arterial 18FDG signal was found to be linked to levels of inflammatory biomarkers[89] and to factors of the metabolic syndrome[90].

SPECT and PET differ in several ways; given its better spatial resolution (4 to 5 mm *vs* 1 to 1.6 cm)[91,92] and its intrinsic capability to quantify biological processes in absolute terms, PET has been used, with 18FDG or translocator protein ligands and choline ligands, in most of the human studies on nuclear imaging of atherosclerosis. Nonetheless, specific SPECT ligands have been used in order to investigate their capabilities of probing various processes of atherosclerosis progression and rupture, including chemotaxis[93], angiogenesis[94], lipoprotein accumulation[95], proteolysis[96] and thrombogenicity[97]. For these reasons, PET and SPECT have been established as important tools for identifying vascular inflammation in the inflammatory vasculitides, and for monitoring patients with inflammatory diseases[98,99].

Specifically, the possibility of imaging *in vivo* early and developing plaque-like lesions by means of a C-type atrial natriuretic factor (C-ANF) has been investigated[100]. Vulnerable lesions are indeed often characterised by vascular remodelling and manifest the up-regulation of natriuretic peptide clearance receptors (NPR-Cs) expression both in the endothelium and in vascular SMCs (VSMCs); natri-

Table 3 Plaque feature identification through invasive diagnostic imaging

	IVUS	VH	US-E	OCT	IVMRI
Morphology features					
Outward remodelling	-[1]	-[1]	[137][1]	[116][1]	-[1]
Plaque burden	[124][1]	-[1]	[137][1]	[116][1]	-[1]
Lipid pool	[126][1]	[130][1]	-[2]	-[1]	-[1]
Necrotic core	[124][1]	[131][1]	-[2]	-[1]	-[1]
Composition					
Fibro-fatty		[131][1]	[141][1]	[116][1]	[146,147][1]
Fibrous plaque		[131][1]	[141][1]	[116][1]	
Dense calcium	[128][1]	[131][1]	[138][1]	[116][1]	
Biological features					
Inflammation	-[2]	[57][1]		[122][1]	-[2]
Macrophage infiltration	-[2]	-[2]	[141][1]	[119][1]	-[2]
Neo-angiogenesis	-[2]	-[2]	-[2]	-[2]	-[2]
TFCA	-[1]	-[1]	-[1]	[116][1]	-[2]
TFCA + MI	-[2]	-[2]	[137][1]	-[2]	-[2]

[1]Limited clinical experience; [2]research in progress. IVUS: Intravascular ultrasound; VH: Virtual histology; OCT: Optical coherence tomography; US-E: Elastography; IVMRI: Intravascular magnetic resonance imaging; MI: Macrophage infiltration; TFCA: Thin fibrous cap atheroma.

uretic peptides have strong antiproliferative and antimigratory effects on VSMCs. C-ANF was functionalised with 1,4,7,10-tetraazacyclododecane-1,4,7,10-tetraacetic acid (DOTA) and labelled with copper-64 (64Cu) then, prior to PET scanning, injected in a hypercholesterolaemic rabbit bearing atherosclerotic-like lesions. Histopathology and immunohistochemistry analyses were performed to assess plaque development and NPR-C localisation. 64Cu-DOTA-C-ANF uptake in the atherosclerotic region was imaged by PET, with the highest target-to-background ratio (3.59 ± 0.94). PET and immunohistochemistry competitive blocking studies confirmed receptor-mediated 64Cu-DOTA-C-ANF uptake in the plaque, concluding that the tracer may be a promising candidate for *in vivo* PET imaging of NPR-Cs on atherosclerotic plaques[100]. Furthermore, monocyte recruitment can be imaged by means of a radiolabelled peptide (18F-4V), which can be internalized by the endothelial cells through VCAM-1-mediated binding[101].

MMPs are also believed to play a crucial role in plaque destabilization; hence the feasibility of *in vivo* imaging of MMP expression has also been investigated. In particular, the results from radiolabelled broad-based MPI administered to apoE null and LDLR null mice described the *in vivo* uptake of a 99mTc-labelled MPI RP805 in aortic atherosclerotic plaque; uptake of the tracer correlated with immunohistochemical staining for macrophages and with MMP-2 and MMP-9[102,103]. Furthermore, modifications in the signal from the 99mTc-MPI within the lesion can be used to tailor therapies, usually statin-based, to reduce MMP expression[104].

However, the main limitation of PET is poor spatial resolution; nonetheless, this difficulty has, to a large extent, been overcome by advances in imaging hardware and software that allow PET images to be co-registered with another imaging modality with much higher spatial resolution (most commonly CT, often in combined PET-CT scanners)[105]. The first clinical study using PET-CT to assess atheromas *in vivo* included 8 patients presenting with angiographic carotid artery stenosis and reporting a recent transient ischemic attack (TIA). PET was co-registered with CT, and plaques were found ipsilaterally with respect to the ischemic symptoms in all patients; furthermore, 18FDG accumulated in the ipsilateral plaque, significantly more than in the plaque on the contralateral side. On the basis of the histological analysis following carotid endarterectomy, areas of 18FDG uptake were found to correspond to dense macrophage infiltration within the plaque[106]. A subsequent larger study confirmed these findings and correlated the degree of 18FDG uptake with the degree of macrophage staining in the corresponding histological sections[107].

PET can also be co-registered with CMR (Figure 6), which provides better plaque imaging; requiring two separate scans, co-registration using anatomical landmarks is needed in this case. In the past, the combination of the two modalities has revealed, for patients with recent TIA and an ipsilateral high-grade carotid stenosis, an additional ipsilateral lesion with a high level of 18FDG uptake, but without high-grade stenosis[108].

PET-CT has also been used to assess the effectiveness of statin therapy in reducing the level of inflammation[109]. More challenging is the imaging of inflamed atheroma in the coronary vasculature with 18F-FDG due to myocardial uptake of 18F-FDG and the smaller size of the coronary arteries. Nonetheless, the feasibility of PET-CT imaging of inflamed lesions in the coronary vessels has been recently demonstrated, suppressing the myocardial 18FDG uptake by administering a high-fat, low-carbohydrate diet to the patients[110].

Alternatively, 18F-labelled fluorocholine (FCH) can be used to elude 18FDG myocardial uptake[111]. FCH is a tracer usually employed to image prostate cancer on the basis that activity of the choline-specific transporter increases in proliferating cells. Activated macrophages, similar to tumour cells, show enhanced FCH uptake[112], and a study conducted on mice demonstrated, for the first time, that FCH has a greater sensitivity in detecting plaques with respect to FDG (84% *vs* 64%)[113].

INVASIVE IMAGING TECHNIQUES

Diagnostic imaging can be used to closely investigate the atherosclerotic lesion due to probe miniaturization which allows intravascular imaging of symptomatic patients, undergoing invasive angiography, in order to detect morphological and biological markers of unstable and vulnerable plaques, as listed in Table 3.

Intravascular optical coherence tomography

Studies have revealed that optical coherence tomography (OCT) is capable of differentiating lipid tissue from water-based tissues[114]. Furthermore, the thickness of the fibrous cap overlying an atheroma can be demarcated by OCT, as demonstrated in the *in vitro* analysis of aortic tis-
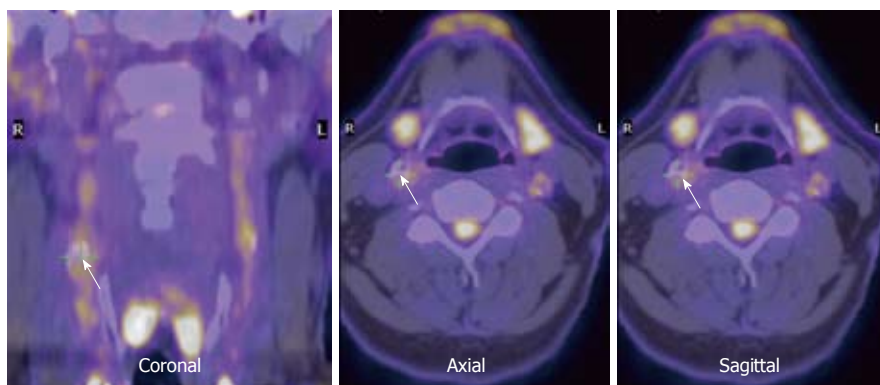
Figure 6 Co-registered fluorodeoxyglucose positron emission tomography and low-resolution magnetic resonance images in the neck region (arrows). Right carotid is indicated (courtesy of Dr. Rudd).
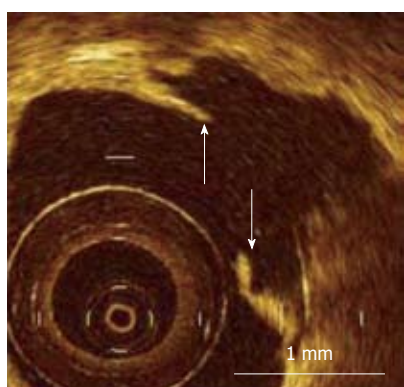
Figure 7 Measurement of fibrous cap thickness in ruptured plaque using optical coherence tomography. Residual fibrous cap was identified as a flap between the lumen of the coronary artery and the cavity of plaque, and its thickness was measured at the thinnest part (arrows). Scale bar = 1 mm (courtesy of Dr. Kubo).

sue[114]. The potential for intravascular assessment of culprit lesions in the coronary arteries has also been investigated. This procedure could enable detailed measurement of fibrous cap thickness as well as identification of erosive processes and thrombus formation, as achievements in post mortem samples have suggested (Figure 7)[115].

Usually performed only qualitatively *via* OCT[116], identification of plaque components amongst fibrous, calcified and lipid-rich tissues is intended to be supported quantitatively by targeting specific optical coefficients, such as optical attenuation μt[117], backscatter and extinction coefficients[118]. OCT can also evaluate the presence and quantity of cellular species typically found in atherosclerotic plaques such as macrophages and smooth muscle actin[119]. The feasibility and accuracy of OCT for detecting the frequency and spatial distribution of TFCA has been investigated on coronary arterial segments *ex vivo*; OCT accurately detected TFCA with 90% sensitivity and 79% specificity[116].

The use of OCT, which has a resolution between 4 and 20 μm, may be advantageous in measuring vulnerable cap thickness, usually thinner than 65 μm, and recent findings demonstrated that quantitative assessment of plaque components could be feasible *in vivo*[120]. The further diagnostic potential of OCT imaging can be seen in the use of functionalized magnetofluorescent NPs tar-

geting endothelial markers, such as VCAM-1 which is a critical component of the leukocyte-endothelial adhesion cascade regulating the atherogenic process[121]. Cathepsin B activated NPs were also used within optical imaging methodologies to monitor plaque inflammation in small animal *in vivo* studies[122].

Clearly, the major limitation of OCT is its invasiveness, limiting its application to patients who have already been referred for X-ray angiography. Nonetheless, OCT remains the imaging technique with the highest spatial resolution, suitable for assessing the thickness of the fibrous cap.

Intravascular ultrasound

US imaging of arterial disease with magnified detail of the plaque has been made possible only since the recent expansion of endovascular techniques and ultrasound probe miniaturization, which has led to the rapidly evolving diagnostic imaging modality known as IVUS[123]. IVUS provides real-time, as opposed to offline IB-US processing, with cross-sectional images of the examined vessel perpendicular to the longitudinal axis of the catheter. Previous studies on the applicability of IVUS in conjunction with coronary angiography demonstrated the feasibility of 3D reconstruction of coronary arteries *via* IVUS, with the motion of the catheter being tracked from bi-planar angiographic images[124]. The latest IVUS probes use phased array transducers sited around the tip of a catheter, allowing coaxial and fast exchange catheter configurations with a guide wire. Phased array US employs an electronically-controlled current that travels around the transducer firing US signals, which are sent out in a rotating sweep[125]. An IVUS examination can discriminate all three layers of the arterial wall[126], detect the presence of plaque[127], and can assess atherosclerotic disease[128] as well as plaque features, by identifying vulnerable or ruptured plaques, Glagov-type outward arterial remodelling[129,130] and the extent of calcified nodules, with variable accuracy depending on the regularity of lumen surface (sensitivity 94.1%, specificity 90.3% for convex lumen; sensitivity 64.7%, specificity 88.4% for irregular lumen)[128]. Monitoring changes in the extent of coronary atherosclerosis with IVUS has been increasingly employed in clinical trials to assess progression of the pathology, as IVUS is able to generate high-resolution
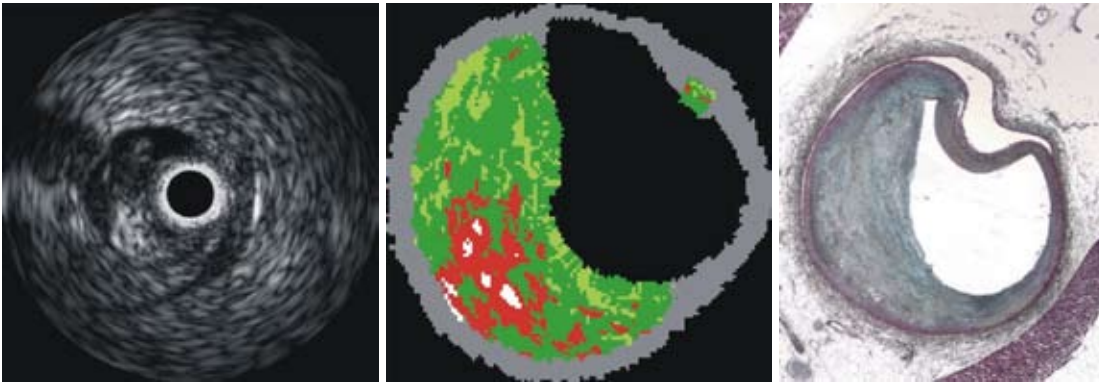
Figure 8 Example of intravascular ultrasound imaging (left), virtual histology (center) and movat pentachrome histology (courtesy of Dr. Nair).

imaging of the entire thickness of the coronary artery wall permitting evaluation of the entire burden of atherosclerotic plaque[131]. The resolution of IVUS (150 to 300 μm) may be insufficient to detect thin fibrous caps in coronary (50 to 75 μm) or carotid arteries (200 μm)[129]. However, "virtual histology" (VH) could be realized through IVUS, implementing the spectral analysis of the backscattering US signal to model plaque in three dimensions. This approach has been validated in *ex vivo* coronary arteries, and was successful in identifying lipid-rich necrotic cores, fibro-fatty plaques, and regions of calcification (Figure 8) with high accuracy[132-134]; additionally, its application *in vivo* demonstrated that the angiographic and clinical outcome up to 12 mo after long stent placement guided by IVUS was superior to guidance by angiography[135].

Despite its invasiveness, IVUS facilitates the *in vivo* delineation of the relative contributions of the necrotic core and fibrous atheroma in unstable lesions. Its clinical potential lies in it being used prior to percutaneous intervention in order to inspect and measure vessel size, evaluate side-branch anatomy, plaque length and assess calcification. Recent studies demonstrated that IVUS employed in conjunction with carotid artery stenting provided precise disease assessment and efficient surgery planning with no adverse events[136]. Although showing satisfactory inter-operator reproducibility, the classification of VH still relies on manual border detection and needs an improved automatic border detection algorithm for the use of VH IVUS as a diagnostic tool for surgical assessment[137].

IVUS can also be employed in elastography (US-E) to determine mechanical properties of the plaque. Elastography reflects the rate of deformation (strain) of the tissue and can be employed as an index of mechanical stiffness. The lumen is strained between pairs of US detectors that acquire the signal at a certain intraluminal pressure and at a slightly different pressure value (± 3 mmHg)[138,139]. Displacement of the signals of the two IVUS images is estimated and the strain of the tissue can be calculated by dividing the differential displacement ("displacement of proximal layer" - "displacement of distal layer") by the undeformed distance between the

two layers. The strain can then be calculated for multiple layers and colour-coded into a so-called "elastogram". The elastogram images the radial strain on the arterial wall and plaque deformability can be derived for the entire volume (Figure 9). Specifically, US-E showed a high sensitivity and specificity (88% and 89%) in identifying vulnerable plaques from excised human coronary arteries[140]. Moreover, animal studies demonstrated that elastography is capable of identifying fibro-fatty and fibrous plaques and macrophage infiltration, with high sensitivity (93%, 96% and 92%, respectively) and specificity (89%, 76% and 66%, respectively)[141].

Although US-E is able to differentiate fatty from fibrous plaques, compared with VH-IVUS, it remains an emerging imaging modality, thus prospective studies correlating vulnerable plaques identified by US-E and cardiac events are underway[142].

Intravascular MRI
Similar to IVUS, probe miniaturization allowed the development of intravascular MRI (IVMRI) catheters capable of imaging the arterial wall of the aorta or the coronary arteries without external magnets or coils, and the resulting signal enabled the differentiation of lipid-rich and fibrotic-rich areas of the atherosclerotic plaque on the basis of differential water diffusion[143-145]. Preliminary *ex vivo* studies demonstrated good agreement between IVMRI and histology, with a specificity of 89% and a sensitivity of 100%, with spatial resolution of IVMRI as low as 100 μm[146]. Regardless of the limitations due to the necessary use of an occluding balloon and to the mechanical rotation of the catheter, *in vivo* data obtained in human iliac arteries indicate that IVMRI might be superior to IVUS in identifying lipid, fibrous and calcified areas within the plaque burden[147].

CONCLUSION
Clinical results obtained by exploiting the capabilities derived from efficient plaque imaging show how current guidelines for atherosclerosis therapy planning, based purely on percentage stenosis, fail to address a significant proportion of culprit lesions. Therefore, medical imag-
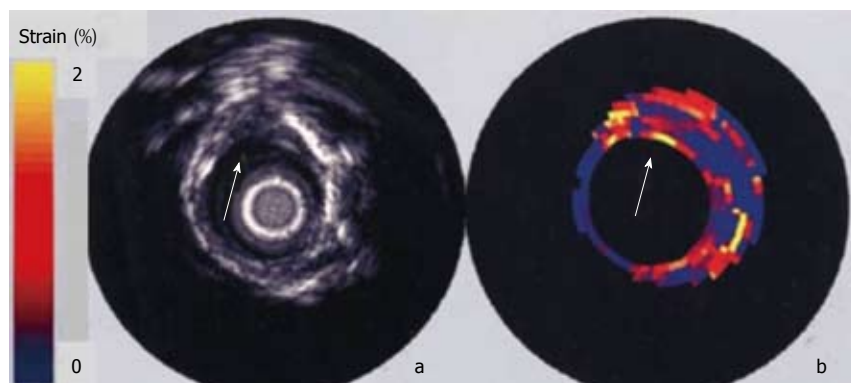
Figure 9 *In vitro* **intravascular echogram and elastogram of a human femoral artery.** The elastogram reveals that the plaque at 12 o'clock contains a soft core that is covered from the lumen by a stiff cap. At 9 o'clock a soft tissue is present at the lumen vessel-wall boundary. A different strain was found at 9 and 3 o'clock and this difference was not present in the echogram[140].
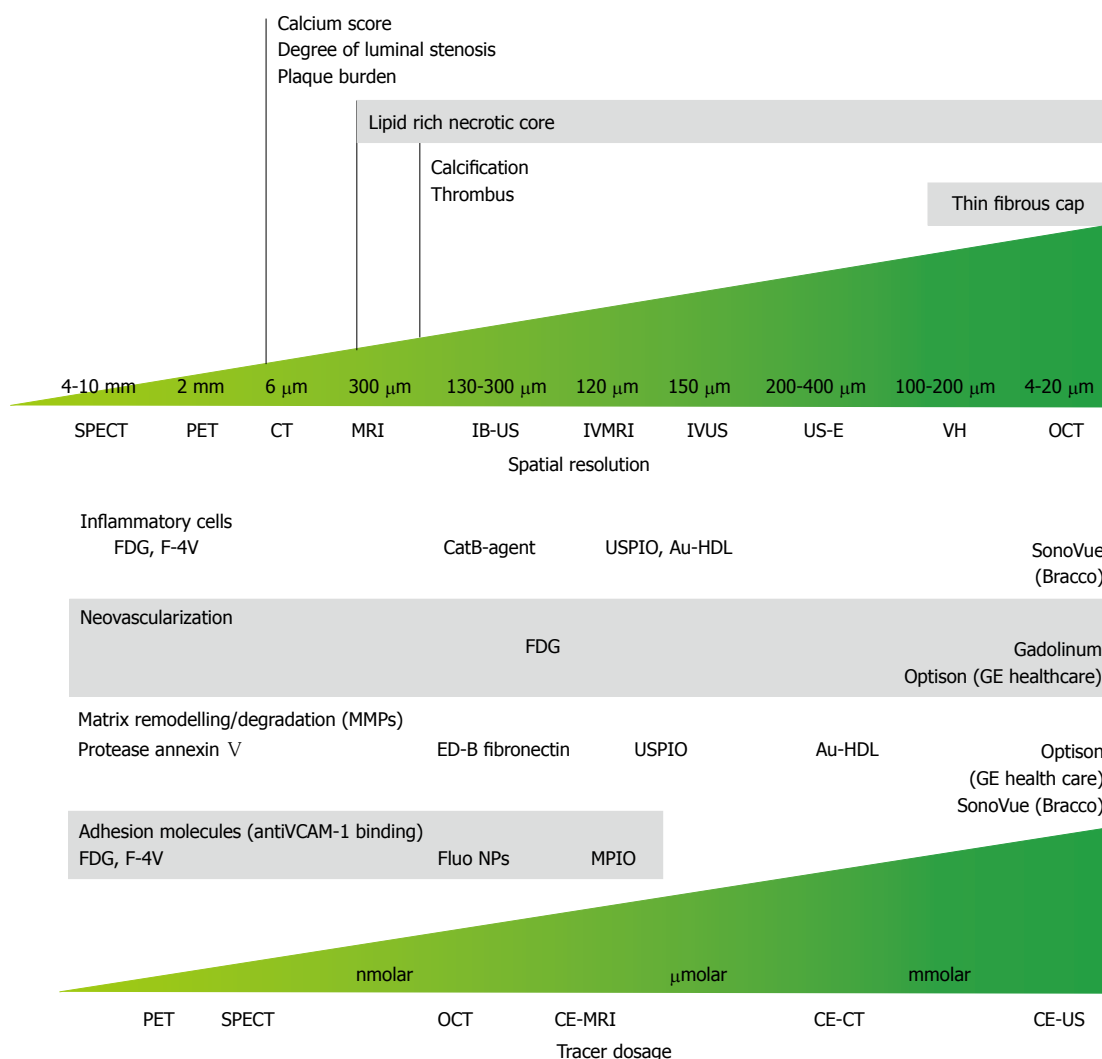
**Figure 10 Spatial resolution and dose-effectiveness of different diagnostic imaging modalities.** Minimum spatial resolution required for the identification of the indicated morphological feature of vulnerable atherosclerotic plaque (top); dose effectiveness in the identification of specific biological processes and compound; specific target and respective tracer are indicated (bottom). SPECT: Single photon emission computed tomography; PET: Positron emission tomography; CT: Computed tomography; MRI: Magnetic resonance imaging; IB-US: Integrated backscatter ultrasonography; IVMRI: Intravascular magnetic resonance imaging; IVUS: Intravascular ultrasound; US-E: Intravascular ultrasound employed in elastography; VH: Virtual histology; OCT: Optical coherence tomography; CE-MRI: Contrast-enhanced magnetic resonance imaging; CE-CT: Contrast-enhanced computed tomography; CE-US: Contrast-enhanced ultrasonography; FDG: Fluorodeoxyglucose; USPIO: Ultra-small super paramagnetic iron oxide; Au-HDL: High-density lipoprotein nanoparticle contrast agent; VCAM: Vascular cell adhesion molecule; NP: Nanoparticle; MPIO: Microparticles of iron oxide.

ing is continuously improving towards higher accuracy in recognizing *in vivo* morphological and molecular features related to vulnerability. Specifically, identification of morphological features is more effective with higher spatial resolved imaging modalities (Figure 10, top), whereas precise biological processes and compound detection is achievable independent of the spatial resolution of imaging modalities able to trace the specific contrast agent and

Clinically available

| US | PET | CT | MRI | OCT | IVUS |

Preclinical stage

| CE-US IB-US | | CE-CT | | | VH US-E |

Experimental stage

| PET-MRI | PET-CT | CE-MRI |
| Novel PET tracer | | IVMRI |
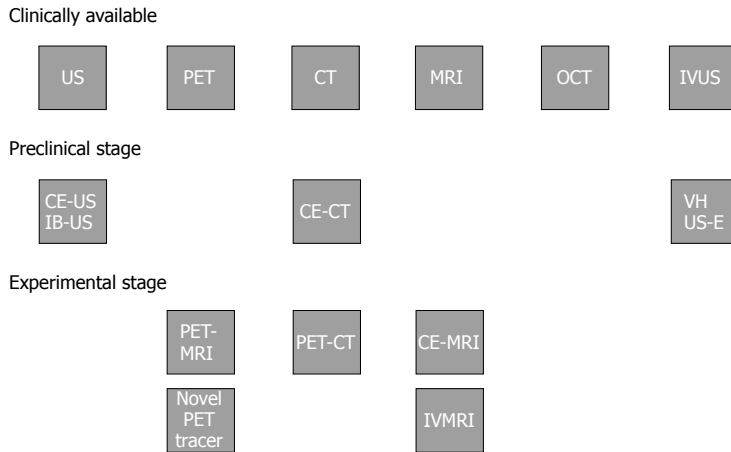
Figure 11 Clinical implementation and research status of diagnostic imaging modalities for atherosclerotic plaque characterization. US: Ultrasonography; PET: Positron emission tomography; CT: Computed tomography; MRI: Magnetic resonance imaging; OCT: Optical coherence tomography; IVUS: Intravascular ultrasound; VH: Virtual histology; US-E: Intravascular ultrasound employed in elastography; CE-US: Contrast-enhanced ultrasonography; IB-US: Integrated backscatter ultrasonography; CE-CT: Contrast-enhanced computed tomography; PET-MRI: Positron emission tomography-magnetic resonance imaging; PET-CT: Positron emission tomography-computed tomography; CE-MRI: Contrast-enhanced-magnetic resonance imaging; IVMRI: Intravascular magnetic resonance imaging.

is considered highly efficient for minimum agent dose administration (Figure 10, bottom).

Current challenges for atherosclerosis plaque imaging

The *in vivo* detection of plaque vulnerability has the potential to become a reality soon, due to the various techniques described in this review, when they are translated into the clinical routine. However, their implementation is currently limited by the difficulty in resolving minute regions of interest within a much larger field of view, for instance when small coronary vessel diameter is below PET and SPECT spatial resolution. Presentation of the information in a quantifiable and easy-to-read manner also needs further improvements to achieve effective employment in the diagnostic paradigm.

Moreover, the correlation between imaging data, the risk of rupture and, eventually, the outcome of patients needs to be reinforced, broadening what was recently addressed by VH and IVUS based clinical trials[148,149] through the collection of blood-based markers and diverse imaging data. Therefore, novel techniques need to be widely available and affordable to allow the success of ongoing prospective studies[150] and to provide standardized high-quality image sets for quantitative reference, as well as new integrated risk markers for low-risk and intermediate-risk population management.

Future perspective

A summary of the clinical implementation and research stage of the different imaging modalities is illustrated in Figure 11.

Potential advances in image based plaque morphology assessment can be seen from the application of 3T and 7T MR scanners in clinical practice, as documented in a recent study[151] as well as from the implementation in real-time of IB-US methodologies and RF spectral analyses. Furthermore, implementation of micro and nanostructured contrast agents, developed to selectively

enhance specific biological compounds at a molecular level, could lead to a substantial reduction in contrast agent dose to achieve satisfactory examinations[11,43].

Further improvements in available imaging modalities should take account of the costs that would be incurred once implemented and the trade-off in terms of diagnostic accuracy (Figure 12); those requiring a catheterization procedure are not only highly invasive, hence useful for a niche of symptomatic cases already referred for arterial angiography, but are extremely expensive as the catheterization intervention increases the cost of these imaging modalities to 20 times more than US and double that of the most expensive non-invasive imaging modality[152]. The latter, PET, is a concern due to the radioactive nature of 18FDG, as each examination has a radiation exposure of approximately 5 mSv (250 chest X ray equivalents)[153]. Therefore, clinical translation of novel contrast media for CT and MRI as well as the development of innovative sequencing may allow a similar level of accuracy with limited costs; additionally, improvements in CE-US and further optimization towards real-time implementation of IB-US analysis will result not only in a drastic reduction in costs associated with plaque characterisation, but also an important reduction in the invasiveness of such diagnostic procedures. For example, although their human application is still limited, the optical properties of contrast media suitable for US imaging are being extensively studied[154-156] aimed at a hybrid imaging modality, namely optoacoustic imaging, which could obtain images with high optical contrast at high ultrasonic resolution in relatively large volumes of biological tissue[15,157]. The use of NPs combined with a site specific drug delivery system is extremely promising for pharmacological and gene therapy applications[158] or molecular guided LASER or US based interventions[40]. Finally, implementation of nanostructured contrast agents will reduce the health hazards due to ionizing radiation or radioactive tracers and of those derived from surgical treatments and from
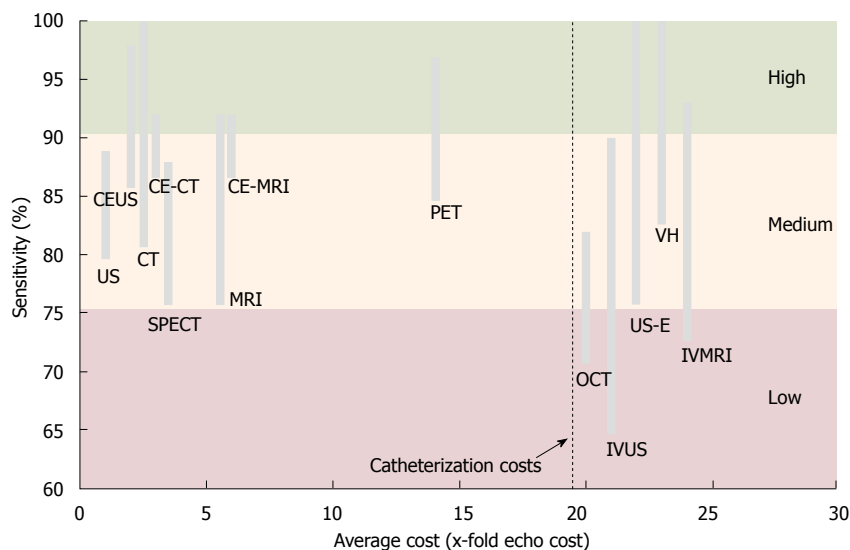
Figure 12 Cost-effectiveness of diagnostic imaging modalities for atherosclerotic plaque characterization. The range of sensitivity is used for accuracy quantification. Echocardiography is the cost comparator where costs of other modalities are a ratio of x-fold higher costs. Indicated intravascular imaging costs add-up catheterization costs (costs are unit operating costs, not charges). CE-US: Contrast-enhanced ultrasonography; CE-CT: Contrast-enhanced computed tomography; CE-MRI: Contrast-enhanced magnetic resonance imaging; CT: Computed tomography; US: Ultrasound; SPECT: Single photon emission computed tomography; MRI: Magnetic resonance imaging; OCT: Optical coherence tomography; IVUS: Intravascular ultrasound; IVMRI: Intravascular magnetic resonance imaging.

traditional high dose pharmacological therapies.

Translating *in vivo* the possibility of performing high resolution imaging and highly accurate reconstruction of plaque components distribution, traditionally performed on histological specimens, may lead to a completely different approach to atherosclerosis assessment and therapeutic planning.

REFERENCES

1   **Roger VL**, Go AS, Lloyd-Jones DM, Adams RJ, Berry JD, Brown TM, Carnethon MR, Dai S, de Simone G, Ford ES, Fox CS, Fullerton HJ, Gillespie C, Greenlund KJ, Hailpern SM, Heit JA, Ho PM, Howard VJ, Kissela BM, Kittner SJ, Lackland DT, Lichtman JH, Lisabeth LD, Makuc DM, Marcus GM, Marelli A, Matchar DB, McDermott MM, Meigs JB, Moy CS, Mozaffarian D, Mussolino ME, Nichol G, Paynter NP, Rosamond WD, Sorlie PD, Stafford RS, Turan TN, Turner MB, Wong ND, Wylie-Rosett J. Heart disease and stroke statistics--2011 update: a report from the American Heart Association. *Circulation* 2011; **123**: e18-e209

2   **Topol EJ**, Yadav JS. Recognition of the importance of embolization in atherosclerotic vascular disease. *Circulation* 2000; **101**: 570-580

3   **Virmani R**, Burke AP, Kolodgie FD, Farb A. Pathology of the thin-cap fibroatheroma: a type of vulnerable plaque. *J Interv Cardiol* 2003; **16**: 267-272

4   **Harrison DG**, Widder J, Grumbach I, Chen W, Weber M, Searles C. Endothelial mechanotransduction, nitric oxide and vascular inflammation. *J Intern Med* 2006; **259**: 351-363

5   **Davies PF**. Flow-mediated endothelial mechanotransduction. *Physiol Rev* 1995; **75**: 519-560

6   **Li YS**, Haga JH, Chien S. Molecular basis of the effects of shear stress on vascular endothelial cells. *J Biomech* 2005; **38**: 1949-1971

7   **Chatzizisis YS**, Coskun AU, Jonas M, Edelman ER, Feldman CL, Stone PH. Role of endothelial shear stress in the natural history of coronary atherosclerosis and vascular remodeling: molecular, cellular, and vascular behavior. *J Am Coll Cardiol* 2007; **49**: 2379-2393

8   **Spagnoli LG**, Bonanno E, Sangiorgi G, Mauriello A. Role of inflammation in atherosclerosis. *J Nucl Med* 2007; **48**: 1800-1815

9   **Redgrave JN**, Gallagher P, Lovett JK, Rothwell PM. Critical cap thickness and rupture in symptomatic carotid plaques: the oxford plaque study. *Stroke* 2008; **39**: 1722-1729

10   **McCarthy MJ**, Loftus IM, Thompson MM, Jones L, London NJ, Bell PR, Naylor AR, Brindle NP. Angiogenesis and the atherosclerotic carotid plaque: an association between symptomatology and plaque morphology. *J Vasc Surg* 1999; **30**: 261-268

11   **Hamilton AJ**, Huang SL, Warnick D, Rabbat M, Kane B, Nagaraj A, Klegerman M, McPherson DD. Intravascular ultrasound molecular imaging of atheroma components in vivo. *J Am Coll Cardiol* 2004; **43**: 453-460

12   **Fukumoto Y**, Hiro T, Fujii T, Hashimoto G, Fujimura T, Yamada J, Okamura T, Matsuzaki M. Localized elevation of shear stress is related to coronary plaque rupture: a 3-dimensional intravascular ultrasound study with in-vivo color mapping of shear stress distribution. *J Am Coll Cardiol* 2008; **51**: 645-650

13   **Groen HC**, Gijsen FJ, van der Lugt A, Ferguson MS, Hatsukami TS, van der Steen AF, Yuan C, Wentzel JJ. Plaque rupture in the carotid artery is localized at the high shear stress region: a case report. *Stroke* 2007; **38**: 2379-2381

14   **Soloperto G**, Keenan N, Sheppard M, Ohayon J, Wood N, Pennell D, Xu YX. Combined imaging, computational and histological analysis of a ruptured carotid plaque: A patient-specific analysis. *Artery Research* 2010; **4**: 59-65

15   **Massai D**, Soloperto G, Gallo D, Xu XY, Morbiducci U. Shear-induced platelet activation and its relationship with blood flow topology in a numerical model of stenosed carotid bifurcation. *Eur J Mech B Fluids* 2012; **35**: 92-101

16   **Ohayon J**, Finet G, Gharib AM, Herzka DA, Tracqui P, Heroux J, Rioufol G, Kotys MS, Elagha A, Pettigrew RI. Necrotic core thickness and positive arterial remodeling index: emergent biomechanical factors for evaluating the risk of plaque rupture. *Am J Physiol Heart Circ Physiol* 2008; **295**: H717-H727

17   **Richardson PD**, Davies MJ, Born GV. Influence of plaque configuration and stress distribution on fissuring of coronary atherosclerotic plaques. *Lancet* 1989; **2**: 941-944

18   **Sones F**, Shirey E, Proudfit W, Westcott R. Cine-coronary arteriography. *Circulation* 1959; **20**: 773-774

19   **Sones FM**, Shirey EK. Cine coronary arteriography. *Mod Concepts Cardiovasc Dis* 1962; **31**: 735-738

20   **Barratt DC,** Davies AH, Hughes AD, Thom SA, Humphries KN. Accuracy of an electromagnetic three-dimensional ultrasound system for carotid artery imaging. *Ultrasound Med Biol* 2001; **27**: 1421-1425

21   **Simons PC**, Algra A, Bots ML, Grobbee DE, van der Graaf Y. Common carotid intima-media thickness and arterial stiffness: indicators of cardiovascular risk in high-risk patients. The SMART Study (Second Manifestations of ARTerial disease). *Circulation* 1999; **100**: 951-957

22   **Hodis HN**, Mack WJ, LaBree L, Selzer RH, Liu CR, Liu CH, Azen SP. The role of carotid arterial intima-media thickness in predicting clinical coronary events. *Ann Intern Med* 1998; **128**: 262-269

23   **Bots ML**, Hoes AW, Koudstaal PJ, Hofman A, Grobbee DE. Common carotid intima-media thickness and risk of stroke and myocardial infarction: the Rotterdam Study. *Circulation* 1997; **96**: 1432-1437

24   **Touboul PJ**, Prati P, Scarabin PY, Adrai V, Thibout E, Ducimetière P. Use of monitoring software to improve the measurement of carotid wall thickness by B-mode imaging. *J Hypertens Suppl* 1992; **10**: S37-S41

25   **Gutierrez M,** Pilon P, Lage S, Kopel L, Carvalho R, Furuie SS. Automatic measurement of carotid diameter and wall thickness in ultrasound images. *Comput Cardiol* 2002; **29**: 359-362

26   **Liang Q**, Wendelhag I, Wikstrand J, Gustavsson T. A multiscale dynamic programming procedure for boundary detection in ultrasonic artery images. *IEEE Trans Med Imaging* 2000; **19**: 127-142

27   **Tortoli P**, Bambi G, Guidi F, Muchada R. Toward a better quantitative measurement of aortic flow. *Ultrasound Med Biol* 2002; **28**: 249-257

28   **Tortoli P**, Guidi G, Pignoli P. Transverse Doppler spectral analysis for a correct interpretation of flow sonograms. *Ultrasound Med Biol* 1993; 19: 115-121

29   **Morganti T,** Ricci S, Vittone F, Palombo C, Tortoli P. Clinical validation of common carotid artery wall distension assessment based on multigate Doppler processing. *Ultrasound Med Biol* 2005; 31: 937-945

30   **Arnold A,** Taylor P, Poston R, Modaresi K, Padayachee S. An objective method for grading ultrasound images of carotid artery plaques. *Ultrasound Med Biol* 2001; **27**: 1041-1047

31   **Urbani MP**, Picano E, Parenti G, Mazzarisi A, Fiori L, Paterni M, Pelosi G, Landini L. In vivo radiofrequency-based ultrasonic tissue characterization of the atherosclerotic plaque. *Stroke* 1993; **24**: 1507-1512

32   **Kawasaki M,** Takatsu H, Noda T, Ito Y, Kunishima A, Arai M, Nishigaki K, Takemura G, Morita N, Minatoguchi S, Fujiwara H. Noninvasive quantitative tissue characterization and two-dimensional color-coded map of human atherosclerotic lesions using ultrasound integrated backscatter: comparison between histology and integrated backscatter images. *J Am Coll Cardiol* 2001; **38**: 486-492

33   **Dunmore BJ**, McCarthy MJ, Naylor AR, Brindle NP. Carotid plaque instability and ischemic symptoms are linked to immaturity of microvessels within plaques. *J Vasc Surg* 2007; **45**: 155-159

34   **Lindner JR**. Molecular imaging of cardiovascular disease with contrast-enhanced ultrasonography. *Nat Rev Cardiol* 2009; **6**: 475-481

35   **Feinstein SB**. The powerful microbubble: from bench to bedside, from intravascular indicator to therapeutic delivery system, and beyond. *Am J Physiol Heart Circ Physiol* 2004; **287**: H450-H457

36   **Coli S**, Magnoni M, Sangiorgi G, Marrocco-Trischitta MM, Melisurgo G, Mauriello A, Spagnoli L, Chiesa R, Cianflone D, Maseri A. Contrast-enhanced ultrasound imaging of intraplaque neovascularization in carotid arteries: correlation with histology and plaque echogenicity. *J Am Coll Cardiol* 2008; **52**: 223-230

37   **Staub D**, Patel MB, Tibrewala A, Ludden D, Johnson M, Espinosa P, Coll B, Jaeger KA, Feinstein SB. Vasa vasorum and plaque neovascularization on contrast-enhanced carotid ultrasound imaging correlates with cardiovascular disease and past cardiovascular events. *Stroke* 2010; **41**: 41-47

38   **Vicenzini E**, Giannoni MF, Puccinelli F, Ricciardi MC, Altieri M, Di Piero V, Gossetti B, Valentini FB, Lenzi GL. Detection of carotid adventitial vasa vasorum and plaque vascularization with ultrasound cadence contrast pulse sequencing technique and echo-contrast agent. *Stroke* 2007; **38**: 2841-2843

39   **Owen DR**, Shalhoub J, Miller S, Gauthier T, Doryforou O, Davies AH, Leen EL. Inflammation within carotid atherosclerotic plaque: assessment with late-phase contrast-enhanced US. *Radiology* 2010; **255**: 638-644

40   **Chen SC**, Ruan JL, Cheng PW, Chuang YH, Li PC. In vitro evaluation of ultrasound-assisted thrombolysis using a targeted ultrasound contrast agent. *Ultrason Imaging* 2009; **31**: 235-246

41   **Casciaro S**, Conversano F, Ragusa A, Malvindi MA, Franchini R, Greco A, Pellegrino T, Gigli G. Optimal enhancement configuration of silica nanoparticles for ultrasound imaging and automatic detection at conventional diagnostic frequencies. *Invest Radiol* 2010; **45**: 715-724

42   **Malvindi MA,** Greco A, Conversano F, Figuerola A, Corti M, Bonora M, Lascialfari A, Doumari HA, Moscardini M, Cingolani R, Gigli G, Casciaro S, Pellegrino T, Ragusa A. Magnetic/silica nanocomposites as dual-mode contrast agents for combined magnetic resonance imaging and ultrasonography. *Advanced Functional Materials* 2011; **21**: 2548-2555

43   **Quick HH**, Debatin JF, Ladd ME. MR imaging of the vessel wall. *Eur Radiol* 2002; **12**: 889-900

44   **Hayes CE**, Mathis CM, Yuan C. Surface coil phased arrays for high-resolution imaging of the carotid arteries. *J Magn Reson Imaging* 1996; **6**: 109-112

45   **Yuan C**, Murakami JW, Hayes CE, Tsuruda JS, Hatsukami TS, Wildy KS, Ferguson MS, Strandness DE. Phased-array magnetic resonance imaging of the carotid artery bifurcation: preliminary results in healthy volunteers and a patient with atherosclerotic disease. *J Magn Reson Imaging* 1995; **5**: 561-565

46   **Toussaint JF**, Southern JF, Fuster V, Kantor HL. T2-weighted contrast for NMR characterization of human atherosclerosis. *Arterioscler Thromb Vasc Biol* 1995; **15**: 1533-1542

47   **Hatsukami TS**, Ross R, Polissar NL, Yuan C. Visualization of fibrous cap thickness and rupture in human atherosclerotic carotid plaque in vivo with high-resolution magnetic resonance imaging. *Circulation* 2000; **102**: 959-964

48   **Yuan C**, Mitsumori LM, Ferguson MS, Polissar NL, Echelard D, Ortiz G, Small R, Davies JW, Kerwin WS, Hatsukami TS. In vivo accuracy of multispectral magnetic resonance imaging for identifying lipid-rich necrotic cores and intraplaque hemorrhage in advanced human carotid plaques. *Circulation* 2001; **104**: 2051-2056

49   **Yuan C**, Kerwin WS, Yarnykh VL, Cai J, Saam T, Chu B, Takaya N, Ferguson MS, Underhill H, Xu D, Liu F, Hatsukami TS. MRI of atherosclerosis in clinical trials. *NMR Biomed* 2006; **19**: 636-654

50   **Saam T**, Ferguson MS, Yarnykh VL, Takaya N, Xu D, Polissar NL, Hatsukami TS, Yuan C. Quantitative evaluation of carotid plaque composition by in vivo MRI. *Arterioscler Thromb Vasc Biol* 2005; **25**: 234-239

51   **Moody AR**, Murphy RE, Morgan PS, Martel AL, Delay GS, Allder S, MacSweeney ST, Tennant WG, Gladman J, Lowe J, Hunt BJ. Characterization of complicated carotid plaque with magnetic resonance direct thrombus imaging in patients with cerebral ischemia. *Circulation* 2003; **107**: 3047-3052

52   **Singh N**, Moody AR, Gladstone DJ, Leung G, Ravikumar R, Zhan J, Maggisano R. Moderate carotid artery stenosis: MR imaging-depicted intraplaque hemorrhage predicts risk of cerebrovascular ischemic events in asymptomatic men. *Radiology* 2009; **252**: 502-508

53   **Wang J**, Ferguson MS, Balu N, Yuan C, Hatsukami TS,

Börnert P. Improved carotid intraplaque hemorrhage imaging using a slab-selective phase-sensitive inversion-recovery (SPI) sequence. *Magn Reson Med* 2010; **64**: 1332-1340

54   **Kwee RM**, van Oostenbrugge RJ, Prins MH, Ter Berg JW, Franke CL, Korten AG, Meems BJ, van Engelshoven JM, Wildberger JE, Mess WH, Kooi ME. Symptomatic patients with mild and moderate carotid stenosis: plaque features at MRI and association with cardiovascular risk factors and statin use. *Stroke* 2010; **41**: 1389-1393

55   **Wang Q**, Wang Y, Cai J, Cai Y, Ma L, Xu X. Differences of signal evolution of intraplaque hemorrhage and associated stenosis between symptomatic and asymptomatic atherosclerotic carotid arteries: an in vivo high-resolution magnetic resonance imaging follow-up study. *Int J Cardiovasc Imaging* 2010; **26**: 323-332

56   **Bremerich J**, Bilecen D, Reimer P. MR angiography with blood pool contrast agents. *Eur Radiol* 2007; **17**: 3017-3024

57   **Cai J**, Hatsukami TS, Ferguson MS, Kerwin WS, Saam T, Chu B, Takaya N, Polissar NL, Yuan C. In vivo quantitative measurement of intact fibrous cap and lipid-rich necrotic core size in atherosclerotic carotid plaque: comparison of high-resolution, contrast-enhanced magnetic resonance imaging and histology. *Circulation* 2005; **112**: 3437-3444

58   **Sirol M**, Itskovich VV, Mani V, Aguinaldo JG, Fallon JT, Misselwitz B, Weinmann HJ, Fuster V, Toussaint JF, Fayad ZA. Lipid-rich atherosclerotic plaques detected by gadofluorine-enhanced in vivo magnetic resonance imaging. *Circulation* 2004; **109**: 2890-2896

59   **Kerwin W**, Hooker A, Spilker M, Vicini P, Ferguson M, Hatsukami T, Yuan C. Quantitative magnetic resonance imaging analysis of neovasculature volume in carotid atherosclerotic plaque. *Circulation* 2003; **107**: 851-856

60   **Frias JC**, Williams KJ, Fisher EA, Fayad ZA. Recombinant HDL-like nanoparticles: a specific contrast agent for MRI of atherosclerotic plaques. *J Am Chem Soc* 2004; **126**: 16316-16317

61   **Deguchi JO**, Aikawa M, Tung CH, Aikawa E, Kim DE, Ntziachristos V, Weissleder R, Libby P. Inflammation in atherosclerosis: visualizing matrix metalloproteinase action in macrophages in vivo. *Circulation* 2006; **114**: 55-62

62   **Lancelot E**, Amirbekian V, Brigger I, Raynaud JS, Ballet S, David C, Rousseaux O, Le Greneur S, Port M, Lijnen HR, Bruneval P, Michel JB, Ouimet T, Roques B, Amirbekian S, Hyafil F, Vucic E, Aguinaldo JG, Corot C, Fayad ZA. Evaluation of matrix metalloproteinases in atherosclerosis using a novel noninvasive imaging approach. *Arterioscler Thromb Vasc Biol* 2008; **28**: 425-432

63   **Tekabe Y**, Li Q, Luma J, Weisenberger D, Sedlar M, Harja E, Narula J, Johnson LL. Noninvasive monitoring the biology of atherosclerotic plaque development with radiolabeled annexin V and matrix metalloproteinase inhibitor in spontaneous atherosclerotic mice. *J Nucl Cardiol* 2010; **17**: 1073-1081

64   **Trivedi RA**, Mallawarachi C, U-King-Im JM, Graves MJ, Horsley J, Goddard MJ, Brown A, Wang L, Kirkpatrick PJ, Brown J, Gillard JH. Identifying inflamed carotid plaques using in vivo USPIO-enhanced MR imaging to label plaque macrophages. *Arterioscler Thromb Vasc Biol* 2006; **26**: 1601-1606

65   **Tang TY**, Howarth SP, Miller SR, Graves MJ, Patterson AJ, U-King-Im JM, Li ZY, Walsh SR, Brown AP, Kirkpatrick PJ, Warburton EA, Hayes PD, Varty K, Boyle JR, Gaunt ME, Zalewski A, Gillard JH. The ATHEROMA (Atorvastatin Therapy: Effects on Reduction of Macrophage Activity) Study. Evaluation using ultrasmall superparamagnetic iron oxide-enhanced magnetic resonance imaging in carotid disease. *J Am Coll Cardiol* 2009; **53**: 2039-2050

66   **Tang TY**, Moustafa RR, Howarth SP, Walsh SR, Boyle JR, Li ZY, Baron JC, Gillard JH, Warburton EA. Combined PET-FDG and USPIO-enhanced MR imaging in patients with symptomatic moderate carotid artery stenosis. *Eur J Vasc Endovasc Surg* 2008; **36**: 53-55

67   **McAteer MA**, Schneider JE, Ali ZA, Warrick N, Bursill CA, von zur Muhlen C, Greaves DR, Neubauer S, Channon KM,
Choudhury RP. Magnetic resonance imaging of endothelial adhesion molecules in mouse atherosclerosis using dual-targeted microparticles of iron oxide. *Arterioscler Thromb Vasc Biol* 2008; **28**: 77-83

68   **Picano E**, Vano E, Semelka R, Regulla D. The American College of Radiology white paper on radiation dose in medicine: deep impact on the practice of cardiovascular imaging. *Cardiovasc Ultrasound* 2007; **5**: 37

69   **Smith-Bindman R**, Lipson J, Marcus R, Kim KP, Mahesh M, Gould R, Berrington de González A, Miglioretti DL. Radiation dose associated with common computed tomography examinations and the associated lifetime attributable risk of cancer. *Arch Intern Med* 2009; **169**: 2078-2086

70   **Detrano R**, Guerci AD, Carr JJ, Bild DE, Burke G, Folsom AR, Liu K, Shea S, Szklo M, Bluemke DA, O'Leary DH, Tracy R, Watson K, Wong ND, Kronmal RA. Coronary calcium as a predictor of coronary events in four racial or ethnic groups. *N Engl J Med* 2008; **358**: 1336-1345

71   **Sangiorgi G**, Rumberger JA, Severson A, Edwards WD, Gregoire J, Fitzpatrick LA, Schwartz RS. Arterial calcification and not lumen stenosis is highly correlated with atherosclerotic plaque burden in humans: a histologic study of 723 coronary artery segments using nondecalcifying methodology. *J Am Coll Cardiol* 1998; **31**: 126-133

72   **Caussin C**, Ohanessian A, Ghostine S, Jacq L, Lancelin B, Dambrin G, Sigal-Cinqualbre A, Angel CY, Paul JF. Characterization of vulnerable nonstenotic plaque with 16-slice computed tomography compared with intravascular ultrasound. *Am J Cardiol* 2004; **94**: 99-104

73   **Motoyama S**, Sarai M, Harigaya H, Anno H, Inoue K, Hara T, Naruse H, Ishii J, Hishida H, Wong ND, Virmani R, Kondo T, Ozaki Y, Narula J. Computed tomographic angiography characteristics of atherosclerotic plaques subsequently resulting in acute coronary syndrome. *J Am Coll Cardiol* 2009; **54**: 49-57

74   **Schuijf JD**, van der Wall EE, Bax JJ. Lesions without calcium: lessons from CT angiography. *Heart* 2009; **95**: 1038-1040

75   **Ferencik M**, Chan RC, Achenbach S, Lisauskas JB, Houser SL, Hoffmann U, Abbara S, Cury RC, Bouma BE, Tearney GJ, Brady TJ. Arterial wall imaging: evaluation with 16-section multidetector CT in blood vessel phantoms and ex vivo coronary arteries. *Radiology* 2006; **240**: 708-716

76   **Raff GL**, Gallagher MJ, O'Neill WW, Goldstein JA. Diagnostic accuracy of noninvasive coronary angiography using 64-slice spiral computed tomography. *J Am Coll Cardiol* 2005; **46**: 552-557

77   **de Weert TT**, Ouhlous M, Meijering E, Zondervan PE, Hendriks JM, van Sambeek MR, Dippel DW, van der Lugt A. In vivo characterization and quantification of atherosclerotic carotid plaque components with multidetector computed tomography and histopathological correlation. *Arterioscler Thromb Vasc Biol* 2006; **26**: 2366-2372

78   **Cordeiro MA**, Miller JM, Schmidt A, Lardo AC, Rosen BD, Bush DE, Brinker JA, Bluemke DA, Shapiro EP, Lima JA. Non-invasive half millimetre 32 detector row computed tomography angiography accurately excludes significant stenoses in patients with advanced coronary artery disease and high calcium scores. *Heart* 2006; **92**: 589-597

79   **Leber AW**, Knez A, von Ziegler F, Becker A, Nikolaou K, Paul S, Wintersperger B, Reiser M, Becker CR, Steinbeck G, Boekstegers P. Quantification of obstructive and nonobstructive coronary lesions by 64-slice computed tomography: a comparative study with quantitative coronary angiography and intravascular ultrasound. *J Am Coll Cardiol* 2005; **46**: 147-154

80   **Komatsu S**, Hirayama A, Omori Y, Ueda Y, Mizote I, Fujisawa Y, Kiyomoto M, Higashide T, Kodama K. Detection of coronary plaque by computed tomography with a novel plaque analysis system, 'Plaque Map', and comparison with intravascular ultrasound and angioscopy. *Circ J* 2005; **69**: 72-77

81   **Hyafil F**, Cornily JC, Rudd JH, Machac J, Feldman LJ, Fayad

ZA. Quantification of inflammation within rabbit atherosclerotic plaques using the macrophage-specific CT contrast agent N1177: a comparison with 18F-FDG PET/CT and histology. *J Nucl Med* 2009; **50**: 959-965

82   **Cormode DP**, Roessl E, Thran A, Skajaa T, Gordon RE, Schlomka JP, Fuster V, Fisher EA, Mulder WJ, Proksa R, Fayad ZA. Atherosclerotic plaque composition: analysis with multicolor CT and targeted gold nanoparticles. *Radiology* 2010; **256**: 774-782

83   **Bulte JW**. Science to practice: can CT be performed for multicolor molecular imaging? *Radiology* 2010; **256**: 675-676

84   **Shapiro BP**, Young PM, Kantor B, Choe YH, McCollough CH, Gerber TC. Radiation dose reduction in CT coronary angiography. *Curr Cardiol Rep* 2010; **12**: 59-67

85   **Einstein AJ**, Elliston CD, Arai AE, Chen MY, Mather R, Pearson GD, Delapaz RL, Nickoloff E, Dutta A, Brenner DJ. Radiation dose from single-heartbeat coronary CT angiography performed with a 320-detector row volume scanner. *Radiology* 2010; **254**: 698-706

86   **Lehman SJ**, Schlett CL, Bamberg F, Lee H, Donnelly P, Shturman L, Kriegel MF, Brady TJ, Hoffmann U. Assessment of coronary plaque progression in coronary computed tomography angiography using a semiquantitative score. *JACC Cardiovasc Imaging* 2009; **2**: 1262-1270

87   **Meijboom WB**, Mollet NR, Van Mieghem CA, Weustink AC, Pugliese F, van Pelt N, Cademartiri F, Vourvouri E, de Jaegere P, Krestin GP, de Feyter PJ. 64-Slice CT coronary angiography in patients with non-ST elevation acute coronary syndrome. *Heart* 2007; **93**: 1386-1392

88   **Rudd JH**, Warburton EA, Fryer TD, Jones HA, Clark JC, Antoun N, Johnström P, Davenport AP, Kirkpatrick PJ, Arch BN, Pickard JD, Weissberg PL. Imaging atherosclerotic plaque inflammation with [18F]-fluorodeoxyglucose positron emission tomography. *Circulation* 2002; **105**: 2708-2711

89   **Wu YW**, Kao HL, Chen MF, Lee BC, Tseng WY, Jeng JS, Tzen KY, Yen RF, Huang PJ, Yang WS. Characterization of plaques using 18F-FDG PET/CT in patients with carotid atherosclerosis and correlation with matrix metalloproteinase-1. *J Nucl Med* 2007; **48**: 227-233

90   **Tahara N**, Kai H, Yamagishi S, Mizoguchi M, Nakaura H, Ishibashi M, Kaida H, Baba K, Hayabuchi N, Imaizumi T. Vascular inflammation evaluated by [18F]-fluorodeoxyglucose positron emission tomography is associated with the metabolic syndrome. *J Am Coll Cardiol* 2007; **49**: 1533-1539

91   **Davies JR**, Rudd JH, Weissberg PL, Narula J. Radionuclide imaging for the detection of inflammation in vulnerable plaques. *J Am Coll Cardiol* 2006; **47**: C57-C68

92   **Rudd JH**, Myers KS, Bansilal S, Machac J, Woodward M, Fuster V, Farkouh ME, Fayad ZA. Relationships among regional arterial inflammation, calcification, risk factors, and biomarkers: a prospective fluorodeoxyglucose positron-emission tomography/computed tomography imaging study. *Circ Cardiovasc Imaging* 2009; **2**: 107-115

93   **Ohtsuki K**, Hayase M, Akashi K, Kopiwoda S, Strauss HW. Detection of monocyte chemoattractant protein-1 receptor expression in experimental atherosclerotic lesions: an autoradiographic study. *Circulation* 2001; **104**: 203-208

94   **Haubner R**. Alphavbeta3-integrin imaging: a new approach to characterise angiogenesis? *Eur J Nucl Med Mol Imaging* 2006; **33** Suppl 1: 54-63

95   **Virgolini I**, Rauscha F, Lupattelli G, Angelberger P, Ventura A, O'Grady J, Sinzinger H. Autologous low-density lipoprotein labelling allows characterization of human atherosclerotic lesions in vivo as to presence of foam cells and endothelial coverage. *Eur J Nucl Med* 1991; **18**: 948-951

96   **Choudhary S**, Higgins CL, Chen IY, Reardon M, Lawrie G, Vick GW, Karmonik C, Via DP, Morrisett JD. Quantitation and localization of matrix metalloproteinases and their inhibitors in human carotid endarterectomy tissues. *Arterioscler Thromb Vasc Biol* 2006; **26**: 2351-2358

97   **Greco C**, Di Loreto M, Ciavolella M, Banci M, Taurino M, Cerquetani E, Chiavarelli R, Naro F, Cusella-De Angelis G, Mele A. Immunodetection of human atherosclerotic plaque with 125I-labeled monoclonal antifibrin antibodies. *Atherosclerosis* 1993; **100**: 133-139

98   **Webb M**, Chambers A, AL-Nahhas A, Mason JC, Maudlin L, Rahman L, Frank J. The role of 18F-FDG PET in characterising disease activity in Takayasu arteritis. *Eur J Nucl Med Mol Imaging* 2004; **31**: 627-634

99   **Kaufmann BA**, Lindner JR. Molecular imaging with targeted contrast ultrasound. *Curr Opin Biotechnol* 2007; **18**: 11-16

100   **Nahrendorf M**, Keliher E, Panizzi P, Zhang H, Hembrador S, Figueiredo JL, Aikawa E, Kelly K, Libby P, Weissleder R. 18F-4V for PET-CT imaging of VCAM-1 expression in atherosclerosis. *JACC Cardiovasc Imaging* 2009; **2**: 1213-1222

101   **Liu Y**, Abendschein D, Woodard GE, Rossin R, McCommis K, Zheng J, Welch MJ, Woodard PK. Molecular imaging of atherosclerotic plaque with (64)Cu-labeled natriuretic peptide and PET. *J Nucl Med* 2010; **51**: 85-91

102   **Ohshima S**, Petrov A, Fujimoto S, Zhou J, Azure M, Edwards DS, Murohara T, Narula N, Tsimikas S, Narula J. Molecular imaging of matrix metalloproteinase expression in atherosclerotic plaques of mice deficient in apolipoprotein e or low-density-lipoprotein receptor. *J Nucl Med* 2009; **50**: 612-617

103   **Kolodgie FD**, Petrov A, Virmani R, Narula N, Verjans JW, Weber DK, Hartung D, Steinmetz N, Vanderheyden JL, Vannan MA, Gold HK, Reutelingsperger CP, Hofstra L, Narula J. Targeting of apoptotic macrophages and experimental atheroma with radiolabeled annexin V: a technique with potential for noninvasive imaging of vulnerable plaque. *Circulation* 2003; **108**: 3134-3139

104   **Fujimoto S**, Hartung D, Ohshima S, Edwards DS, Zhou J, Yalamanchili P, Azure M, Fujimoto A, Isobe S, Matsumoto Y, Boersma H, Wong N, Yamazaki J, Narula N, Petrov A, Narula J. Molecular imaging of matrix metalloproteinase in atherosclerotic lesions: resolution with dietary modification and statin therapy. *J Am Coll Cardiol* 2008; **52**: 1847-1857

105   **Davies JR**, Rudd JH, Weissberg PL, Narula J. Radionuclide imaging for the detection of inflammation in vulnerable plaques. *J Am Coll Cardiol* 2006; **47**: C57-C68

106   **Rudd JH**, Warburton EA, Fryer TD, Jones HA, Clark JC, Antoun N, Johnström P, Davenport AP, Kirkpatrick PJ, Arch BN, Pickard JD, Weissberg PL. Imaging atherosclerotic plaque inflammation with [18F]-fluorodeoxyglucose positron emission tomography. *Circulation* 2002; **105**: 2708-2711

107   **Tawakol A**, Migrino RQ, Bashian GG, Bedri S, Vermylen D, Cury RC, Yates D, LaMuraglia GM, Furie K, Houser S, Gewirtz H, Muller JE, Brady TJ, Fischman AJ. In vivo 18F-fluorodeoxyglucose positron emission tomography imaging provides a noninvasive measure of carotid plaque inflammation in patients. *J Am Coll Cardiol* 2006; **48**: 1818-1824

108   **Davies JR**, Rudd JH, Fryer TD, Graves MJ, Clark JC, Kirkpatrick PJ, Gillard JH, Warburton EA, Weissberg PL. Identification of culprit lesions after transient ischemic attack by combined 18F fluorodeoxyglucose positron-emission tomography and high-resolution magnetic resonance imaging. *Stroke* 2005; **36**: 2642-2647

109   **Tahara N**, Kai H, Ishibashi M, Nakaura H, Kaida H, Baba K, Hayabuchi N, Imaizumi T. Simvastatin attenuates plaque inflammation: evaluation by fluorodeoxyglucose positron emission tomography. *J Am Coll Cardiol* 2006; **48**: 1825-1831

110   **Wykrzykowska J**, Lehman S, Williams G, Parker JA, Palmer MR, Varkey S, Kolodny G, Laham R. Imaging of inflamed and vulnerable plaque in coronary arteries with 18F-FDG PET/CT in patients with suppression of myocardial uptake using a low-carbohydrate, high-fat preparation. *J Nucl Med* 2009; **50**: 563-568

111   **Roivainen A**, Yli-Kerttula T. Whole-body distribution of (11)C-choline and uptake in knee synovitis. *Eur J Nucl Med Mol Imaging* 2006; **33**: 1372-1373

112   **Boggs KP**, Rock CO, Jackowski S. Lysophosphatidylcholine and 1-O-octadecyl-2-O-methyl-rac-glycero-3-phosphocholine inhibit the CDP-choline pathway of phosphatidylcholine

synthesis at the CTP: phosphocholine cytidylyltransferase step. *J Biol Chem* 1995; **270**: 7757-7764

113   **Matter CM**, Wyss MT, Meier P, Späth N, von Lukowicz T, Lohmann C, Weber B, Ramirez de Molina A, Lacal JC, Ametamey SM, von Schulthess GK, Lüscher TF, Kaufmann PA, Buck A. 18F-choline images murine atherosclerotic plaques ex vivo. *Arterioscler Thromb Vasc Biol* 2006; **26**: 584-589

114   **Brezinski ME**, Tearney GJ, Bouma BE, Izatt JA, Hee MR, Swanson EA, Southern JF, Fujimoto JG. Optical coherence tomography for optical biopsy. Properties and demonstration of vascular pathology. *Circulation* 1996; **93**: 1206-1213

115   **Kubo T**, Imanishi T, Takarada S, Kuroi A, Ueno S, Yamano T, Tanimoto T, Matsuo Y, Masho T, Kitabata H, Tsuda K, Tomobuchi Y, Akasaka T. Assessment of culprit lesion morphology in acute myocardial infarction: ability of optical coherence tomography compared with intravascular ultrasound and coronary angioscopy. *J Am Coll Cardiol* 2007; **50**: 933-939

116   **Yabushita H**, Bouma BE, Houser SL, Aretz HT, Jang IK, Schlendorf KH, Kauffman CR, Shishkov M, Kang DH, Halpern EF, Tearney GJ. Characterization of human atherosclerosis by optical coherence tomography. *Circulation* 2002; **106**: 1640-1645

117   **Levitz D**, Thrane L, Frosz M, Andersen P, Andersen C, Andersson-Engels S, Valanciunaite J, Swartling J, Hansen P. Determination of optical scattering properties of highly-scattering media in optical coherence tomography images. *Opt Express* 2004; **12**: 249-259

118   **Xu C**, Schmitt JM, Carlier SG, Virmani R. Characterization of atherosclerosis plaques by measuring both backscattering and attenuation coefficients in optical coherence tomography. *J Biomed Opt* 2008; **13**: 034003

119   **Tearney GJ,** Yabushita H, Houser SL, Aretz HT, Jang IK, Schlendorf KH, Kauffman CR, Shishkov M, Halpern EF, Bouma BE. Quantification of macrophage content in atherosclerotic plaques by optical coherence tomography. *Circulation* 2003; **107**: 113-119

120   **van Soest G**, Goderie T, Regar E, Koljenović S, van Leenders GL, Gonzalo N, van Noorden S, Okamura T, Bouma BE, Tearney GJ, Oosterhuis JW, Serruys PW, van der Steen AF. Atherosclerotic tissue characterization in vivo by optical coherence tomography attenuation imaging. *J Biomed Opt* 2010; **15**: 011105

121   **Kelly KA**, Allport JR, Tsourkas A, Shinde-Patil VR, Josephson L, Weissleder R. Detection of vascular adhesion molecule-1 expression using a novel multimodal nanoparticle. *Circ Res* 2005; **96**: 327-336

122   **Kim DE**, Kim JY, Schellingerhout D, Shon SM, Jeong SW, Kim EJ, Kim WK. Molecular imaging of cathepsin B proteolytic enzyme activity reflects the inflammatory component of atherosclerotic pathology and can quantitatively demonstrate the antiatherosclerotic therapeutic effects of atorvastatin and glucosamine. *Mol Imaging* 2009; **8**: 291-301

123   **Nishanian G**, Kopchok GE, Donayre CE, White RA. The impact of intravascular ultrasound (IVUS) on endovascular interventions. *Semin Vasc Surg* 1999; **12**: 285-299

124   **Slager CJ**, Wentzel JJ, Schuurbiers JC, Oomen JA, Kloet J, Krams R, von Birgelen C, van der Giessen WJ, Serruys PW, de Feyter PJ. True 3-dimensional reconstruction of coronary arteries in patients by fusion of angiography and IVUS (ANGUS) and its quantitative validation. *Circulation* 2000; **102**: 511-516

125   **Rodriguez-Granillo GA**, McFadden EP, Aoki J, van Mieghem CA, Regar E, Bruining N, Serruys PW. In vivo variability in quantitative coronary ultrasound and tissue characterization measurements with mechanical and phased-array catheters. *Int J Cardiovasc Imaging* 2006; **22**: 47-53

126   **DeMaria AN**, Narula J, Mahmud E, Tsimikas S. Imaging vulnerable plaque by ultrasound. *J Am Coll Cardiol* 2006; **47**: C32-C39

127   **Di Mario C**, The SH, Madretsma S, van Suylen RJ, Wilson RA, Bom N, Serruys PW, Gussenhoven EJ, Roelandt JR. De-

tection and characterization of vascular lesions by intravascular ultrasound: an in vitro study correlated with histology. *J Am Soc Echocardiogr* 1992; **5**: 135-146

128   **Popma J.** Coronary angiography and intravascular ultrasound imaging. In: Zipes D, Libby P, Bonow R, Braunwald E, eds. Braunwald's heart disease: a textbook of cardiovascular medicine. 7th ed. Philadelphia: Elsevier Saunders, 2005

129   **Prati F**, Arbustini E, Labellarte A, Dal Bello B, Sommariva L, Mallus MT, Pagano A, Boccanelli A. Correlation between high frequency intravascular ultrasound and histomorphology in human coronary arteries. *Heart* 2001; **85**: 567-570

130   **Maehara A**, Mintz GS, Bui AB, Walter OR, Castagna MT, Canos D, Pichard AD, Satler LF, Waksman R, Suddath WO, Laird JR, Kent KM, Weissman NJ. Morphologic and angiographic features of coronary plaque rupture detected by intravascular ultrasound. *J Am Coll Cardiol* 2002; **40:** 904-910

131   **Mintz GS,** Garcia-Garcia HM, Nicholls SJ, Weissman NJ, Bruining N, Crowe T, Tardif JC, Serruys PW. Clinical expert consensus document on standards for acquisition, measurement and reporting of intravascular ultrasound regression/progression studies. *EuroIntervention* 2011; **6:** 1123-1130,1139

132   **Nair A**, Kuban BD, Tuzcu EM, Schoenhagen P, Nissen SE, Vince DG. Coronary plaque classification with intravascular ultrasound radiofrequency data analysis. *Circulation* 2002; **106**: 2200-2206

133   **Murashige A**, Hiro T, Fujii T, Imoto K, Murata T, Fukumoto Y, Matsuzaki M. Detection of lipid-laden atherosclerotic plaque by wavelet analysis of radiofrequency intravascular ultrasound signals: in vitro validation and preliminary in vivo application. *J Am Coll Cardiol* 2005; **45**: 1954-1960

134   **Nair A**, Margolis MP, Kuban BD, Vince DG. Automated coronary plaque characterisation with intravascular ultrasound backscatter: ex vivo validation. *EuroIntervention* 2007; **3**: 113-120

135   **Oemrawsingh PV**, Mintz GS, Schalij MJ, Zwinderman AH, Jukema JW, van der Wall EE. Intravascular ultrasound guidance improves angiographic and clinical outcome of stent implantation for long coronary artery stenoses: final results of a randomized comparison with angiographic guidance (TULIP Study). *Circulation* 2003; **107:** 62-67

136   **Bandyk DF,** Armstrong PA. Use of intravascular ultrasound as a "Quality Control" technique during carotid stent-angioplasty: are there risks to its use? *J Cardiovasc Surg* (Torino) 2009; **50:** 727-733

137   **Siewiorek GM,** Loghmanpour NA, Winston BM, Wholey MH, Finol EA. Reproducibility of IVUS border detection for carotid atherosclerotic plaque assessment. *Med Eng Phys* 2012; **34:** 702-708

138   **Céspedes I**, Ophir J, Ponnekanti H, Maklad N. Elastography: elasticity imaging using ultrasound with application to muscle and breast in vivo. *Ultrason Imaging* 1993; **15**: 73-88

139   **Ophir J,** Céspedes I, Ponnekanti H, Yazdi Y, Li X. Elastography: a quantitative method for imaging the elasticity of biological tissues. *Ultrason Imaging* 1991; **13**: 111-134

140   **Schaar JA**, De Korte CL, Mastik F, Strijder C, Pasterkamp G, Boersma E, Serruys PW, Van Der Steen AF. Characterizing vulnerable plaque features with intravascular elastography. *Circulation* 2003; **108**: 2636-2641

141   **Zhang PF**, Su HJ, Zhang M, Li JF, Liu CX, Ding SF, Miao Y, Chen L, Li XN, Yi X, Zhang Y. Atherosclerotic plaque components characterization and macrophage infiltration identification by intravascular ultrasound elastography based on b-mode analysis: validation in vivo. *Int J Cardiovasc Imaging* 2011; **27**: 39-49

142   **Schaar JA**, Mastik F, Regar E, den Uil CA, Gijsen FJ, Wentzel JJ, Serruys PW, van der Stehen AF. Current diagnostic modalities for vulnerable plaque detection. *Curr Pharm Des* 2007; **13**: 995-1001

143   **Martin AJ**, Plewes DB, Henkelman RM. MR imaging of blood vessels with an intravascular coil. *J Magn Reson Imaging* 1992; **2**: 421-429

144   **Hurst GC**, Hua J, Duerk JL, Cohen AM. Intravascular (cath-

eter) NMR receiver probe: preliminary design analysis and application to canine iliofemoral imaging. *Magn Reson Med* 1992; **24**: 343-357

145 **Ocali O**, Atalar E. Intravascular magnetic resonance imaging using a loopless catheter antenna. *Magn Reson Med* 1997; **37**: 112-118

146 **Schneiderman J**, Wilensky RL, Weiss A, Samouha E, Muchnik L, Chen-Zion M, Ilovitch M, Golan E, Blank A, Flugelman M, Rozenman Y, Virmani R. Diagnosis of thin-cap fibroatheromas by a self-contained intravascular magnetic resonance imaging probe in ex vivo human aortas and in situ coronary arteries. *J Am Coll Cardiol* 2005; **45**: 1961-1969

147 **Larose E**, Yeghiazarians Y, Libby P, Yucel EK, Aikawa M, Kacher DF, Aikawa E, Kinlay S, Schoen FJ, Selwyn AP, Ganz P. Characterization of human atherosclerotic plaques by intravascular magnetic resonance imaging. *Circulation* 2005; **112**: 2324-2331

148 **Stone GW**, Maehara A, Lansky AJ, de Bruyne B, Cristea E, Mintz GS, Mehran R, McPherson J, Farhat N, Marso SP, Parise H, Templin B, White R, Zhang Z, Serruys PW. A prospective natural-history study of coronary atherosclerosis. *N Engl J Med* 2011; **364**: 226-235

149 **Van Mieghem CA**, McFadden EP, de Feyter PJ, Bruining N, Schaar JA, Mollet NR, Cademartiri F, Goedhart D, de Winter S, Granillo GR, Valgimigli M, Mastik F, van der Steen AF, van der Giessen WJ, Sianos G, Backx B, Morel MA, van Es GA, Zalewski A, Serruys PW. Noninvasive detection of subclinical coronary atherosclerosis coupled with assessment of changes in plaque characteristics using novel invasive imaging modalities: the Integrated Biomarker and Imaging Study (IBIS). *J Am Coll Cardiol* 2006; **47**: 1134-1142

150 **Muntendam P**, McCall C, Sanz J, Falk E, Fuster V. The Bio-

Image Study: novel approaches to risk assessment in the primary prevention of atherosclerotic cardiovascular disease--study design and objectives. *Am Heart J* 2010; **160**: 49-57.e1

151 47 **Xue YJ**, Gao PY, Duan Q, Lin Y, Dai CB. Preliminary study of hemodynamic distribution in patient-specific stenotic carotid bifurcation by image-based computational fluid dynamics. *Acta Radiol* 2008; **49**: 558-565

152 **Pennell DJ**, Sechtem UP, Higgins CB, Manning WJ, Pohost GM, Rademakers FE, van Rossum AC, Shaw LJ, Yucel EK. Clinical indications for cardiovascular magnetic resonance (CMR): Consensus Panel report. *J Cardiovasc Magn Reson* 2004; **6**: 727-765

153 **European Commission.** Referral Guidelines for Imaging. Radiation Protection 118. Luxembourg: Office for Official Publications of the European Communities, 2001

154 **Esenaliev R,** Karabutov A, Oraevsky A. Sensitivity of Laser Opto-Acoustic Imaging in Detection of Small Deeply Embedded Tumors. *IEEE J Sel Top Quant* 1999; **5**: 981-988

155 **Tong L**, Wei Q, Wei A, Cheng JX. Gold nanorods as contrast agents for biological imaging: optical properties, surface conjugation and photothermal effects. *Photochem Photobiol* 2009; **85**: 21-32

156 **Dayton PA**, Zhao S, Bloch SH, Schumann P, Penrose K, Matsunaga TO, Zutshi R, Doinikov A, Ferrara KW. Application of ultrasound to selectively localize nanodroplets for targeted imaging and therapy. *Mol Imaging* 2006; **5**: 160-174

157 **Patwari P**, Weissman NJ, Boppart SA, Jesser C, Stamper D, Fujimoto JG, Brezinski ME. Assessment of coronary plaque with optical coherence tomography and high-frequency ultrasound. *Am J Cardiol* 2000; **85**: 641-644

158 **Patel DN**, Bailey SR. Nanotechnology in cardiovascular medicine. *Catheter Cardiovasc Interv* 2007; **69**: 643-654